Noncollinear magnetism in manganese nanostructures

Martin Zelený,[1] Mojmir Šob,[2,3] and Jürgen Hafner[1]
[1]*Faculty of Physics and Center for Computational Materials Science, University of Vienna, Sensengasse 8/12, A-1090 Wien, Austria*
[2]*Department of Chemistry, Faculty of Science, Masaryk University, CZ-611 37 Brno, Czech Republic*
[3]*Institute of Physics of Materials, Academy of Sciences of the Czech Republic, CZ-616 62 Brno, Czech Republic*
(Received 8 July 2009; revised manuscript received 25 August 2009; published 19 October 2009)

We present *ab initio* spin-density-functional calculations of the magnetic properties of Mn nanostructures with a geometry varying between a straight linear wire and a three-dimensional nanorod, including collinear and noncollinear, commensurate and incommensurate magnetic configurations. With decreasing tension along the axis of the nanostructure we find a series of transitions first from a straight to a zigzag wire, then to planar triangular or hexagonal stripes and further to a nanorod consisting of a periodic stacking of distorted octahedra. At local equilibrium all nanostructures are in a high-moment state, with absolute values of the local magnetic moments per atom varying between $3.79\mu_B$ for a straight noncollinear antiferromagnetic Mn monowire, $3.54\mu_B$ for a triangular collinear antiferromagnetic stripe, $3.40\mu_B$ for a hexagonal collinear ferrimagnetic stripe, and $2.96\mu_B$ for an octahedral noncollinear ferrimagnetic nanorod. For all low-dimensional nanostructures except the monowire we find collinear and noncollinear magnetic structures to be energetically nearly degenerate, if the geometric and magnetic degrees of freedom are relaxed simultaneously. The energetic consequences of a modest change in the interatomic distances are comparable to those of a large canting of the magnetic moments. Compression of the nanostructures leads to a decrease in the magnetic moments.

DOI: 10.1103/PhysRevB.80.144414 PACS number(s): 75.75.+a, 64.70.Nd, 73.22.−f, 81.07.Vb

I. INTRODUCTION

From the point of view of its magnetic properties manganese is an extremely interesting material. A Mn atom has an electronic configuration $3d^5s^2$ and according to Hund's rule it has a maximal spin moment of $5\mu_B$ and zero orbital moment. The unfilled d states lie about 2.1 eV above the occupied states and this is the reason why dilute Mn atoms in semiconductors maintain a high magnetic moment and exhibit ferromagnetism.[1] Dilute Mn atoms in a matrix of noble-metal or simple-metal atoms couple through oscillatory Rudermann-Kittel-Kasuya-Yoshida interactions and the competition between ferromagnetic (FM) and antiferromagnetic (AFM) exchange interactions leads to spin-glass behavior,[2,3] with local moments fluctuating around $3.5\mu_B$ in a Cu-Mn spin glass, for example.

In the bulk phases of Mn the tendency to adopt a high-moment state is in conflict with a high bond strength, as expected for a metal with a half-filled d band—short interatomic distances tend to quench magnetism.[4] Solid Mn exists in no less than five allotropic forms with widely different structural and magnetic properties. α-Mn, the most stable polymorph under ambient conditions, crystallizes in a complex body-centered-cubic lattice with 58 atoms per cubic unit cell, it is AFM below a Néel temperature of T_N=95 K.[5] In the AFM phase the crystalline symmetry is reduced from cubic to tetragonal, the magnetic structure is noncollinear with large magnetic moments on certain crystallographic sites and much smaller moments on the remaining positions, some Mn atoms could even be nonmagnetic. Detailed spin-density-functional calculations have demonstrated that the noncollinearity results from frustrated AFM interactions between Mn atoms in triangular motifs with short interatomic distances.[4] In some sense, α-Mn can be considered as an intermetallic compound between strongly magnetic and almost nonmagnetic Mn atoms—this interpretation is also supported by the fact that α-Mn is isostructural to certain intermetallic compounds. Frustration also determines the magnetic properties of β-Mn. It has been suggested that the simple cubic structure of β-Mn with 20 atoms per cell belongs to the class of fully frustrated lattices (such as the pyrochlore structure) where the frustration overcomes any tendency toward magnetic ordering—β-Mn is a spin liquid.[6,7] γ-Mn has a face-centered-cubic structure in the paramagnetic high-temperature phase (stable above 1368 K). The properties of the AFM phase of γ-Mn ($T_N \sim 570$ K) can be inferred by studying face-centered-cubic alloys such as γ-FeMn and extrapolation to zero Fe content[8,9] or by epitaxial growth of γ-Mn on a fcc substrate.[10–12] It has been shown that the paramagnetic to AFM transition always induces a tetragonal distortion and that the sign of the distortion can be positive or negative. Contraction along the tetragonal axis is coupled to layered antiferromagnetism while an expansion along the tetragonal axis is associated with in-plane antiferromagnetism,[8,10–12] in accordance with theoretical predictions.[13,14] Body-centered-cubic Mn is stable only from 1406 K up to the melting point, for the hypothetical magnetically ordered low-temperature phase multiple locally stable incommensurate spin-spiral states have been predicted.[14,15] Finally, a hexagonal close-packed ϵ-Mn phase stabilized under pressure is nonmagnetic.[7,16]

Nanostructures of Mn display a similar complexity. Monolayers and bilayers of Mn grown on W(100) have a FM ground state,[17,18] antiferromagnetism develops only in films with three or more atomic layers. Free-standing square monolayers and monolayers on W(110) substrates are AFM, suggesting that the ferromagnetism observed for Mn/W(100) is substrate-induced. Very recent spin-polarized scanning tunneling microscopy work has modified the picture of Mn/W(100) monolayers. It has been shown that the FM state is modulated by a spin-spiral propagating along the ⟨110⟩ di-

rections. It was suggested that the spin spiral is stabilized by a Dzyaloshinski-Moriya interaction induced by spin-orbit coupling.[19] Monolayers and bilayers of Mn supported on a FM Fe(100) substrate adopt a noncollinear spin-flop phase with the Mn moments oriented roughly perpendicular to the magnetic moments of the substrate,[14,20] arising from the competition between the AFM coupling within the Mn layer and the FM coupling through the Fe/Mn interface.

In square layers AFM ordering is possible without frustration, in contrast to the triangular layers formed on a close-packed (111) fcc surface. For the AFM triangular layer with nearest-neighbor interactions only it has been shown using Monte Carlo simulations that the magnetic ground state has $\sqrt{3}\times\sqrt{3}$ periodicity, with $\pm 120°$ angle between spins on neighboring sites (the Néel phase).[21] *Ab initio* calculations allowing for noncollinear spins lead to a slightly different picture: while Cr/Cu(111) monolayers adopt the expected noncollinear Néel phase, in Mn/Cu(111) a rowwise 2×1 AFM phase is preferred,[22,23] probably because of the long-range nature of the magnetic exchange interactions. Kurz *et al.*[23] discussed also other noncollinear spin structures (including three-dimensional structures) derived from complex spin Hamiltonians but for triangular Mn layers all were found to be higher in energy.

One-dimensional (1D) nanostructures (linear and zigzag chains) have recently been investigated by Tung and Guo[24] and Ataca *et al.*[25] While both groups find an FM ground state for straight and an AFM state for zigzag wires, large differences are reported in the magnetic moments of the antiferromagnetic ground-state configurations. These differences already highlight the difficulties to achieve converged results for magnetic Mn nanostructures. For Mn chains supported on a Ni(100) substrate Lounis *et al.*[26] have reported a surprising even-odd alternation of the magnetic structure: infinite or even-numbered chains of Mn atoms adopt a noncollinear magnetic structure while short chains containing an odd number of atoms have a collinear ferrimagnetic (FI) ground state. For larger odd-numbered chains a transition to a noncollinear state is predicted, for infinite chain length both even- and odd-numbered chains converge to the same noncollinear structure. This surprising observation was attributed to the conflict between the AFM exchange coupling along the chain and the FM coupling between substrate and adatoms. The ratio between the AFM intrachain and the FM interface coupling also determines the transition length for odd-numbered chains. A detailed analysis of these even-odd effects in antiferromagnetic chains within the framework of a nearest-neighbor Heisenberg model was given by Politi and Pini.[27]

For small gas-phase Mn_n clusters with $n=5\rightarrow 22$ Stern-Gerlach deflection experiments have been reported by Knickelbein.[28] The average magnetic moments derived using a Curie-law analysis of the measured deflections vary nonmonotonically with increasing cluster size. The smallest moment ($0.4\mu_B$) was reported for Mn_{19}, the largest moment ($1.7\mu_B$) for Mn_{12}. For the smallest clusters (Mn_5 and Mn_6) a symmetric broadening of the cluster beam was observed and this was interpreted, in the light of density-functional calculations, in terms molecular ferrimagnetism of these clusters. The experiments of Knickelbein have revived an already very strong interest in the theory of the magnetic properties of Mn_n clusters. The spin-density-functional calculations reported so far fall into two broad groups: those considering only collinear magnetic moments[29–45] and those admitting noncollinear orientations of the local magnetic moments.[46–52] Even for the simplest case of an Mn_2 dimer both FM (Refs. 30, 34, and 39) and AFM (Refs. 29, 38, and 40) solutions have been reported. Comprehensive discussions of the dimer case have been given very recently by Mejia-Lopez *et al.*[52] within density-functional theory (DFT) and by Tzeli *et al.*[44] on the basis of multireference Hartree-Fock (MR-HF) theory. Both approaches lead to the conclusion that locally stable FM and AFM solutions with bond lengths differing by about 0.3 Å coexist. The change in sign in the magnetic exchange coupling is driven by the different degree of $4s$-$3d$ hybridization varying with the bond length. However, whereas DFT predicts the AFM solution at short bond length to be more stable, the MR-HF calculations conclude to the contrary. Tzeli *et al.*[44] also argued that because in the $S=5/2$ state of a Mn atom all $3d$ orbitals are equally occupied, the binding is of a van der Waals type, different spin states of the Mn dimer being essentially degenerate. For clusters with $n\geq 3$ the collinear calculations agree on FM in the smallest clusters (with a magnetic moment per atom equal to $5\mu_B$), changing to FI with increasing cluster size and on a magnetic energy difference between the FM and FI states growing rapidly with cluster size. However, there is disagreement on the magnitudes of the magnetic moments and on the critical size for the FM to FI transition. Nayak *et al.*[31,32] found FM solutions for $n=2-5$, Pederson *et al.*[30] extended the FM solutions to Mn_n with $n=6-8$ with total magnetic moments of $26\mu_B$, $29\mu_B$, and $32\mu_B$, respectively. In contrast, more recent studies reported that already beginning with Mn_5 ferromagnetic and AFM exchange interactions are in competition and the ground state is FI (Refs. 33–35, 37, 39, 43, and 45). However, although all these studies have been performed within the generalized-gradient approximation of DFT, the magnetic moments for the ground-state configurations differ widely. For Mn_6 the total magnetic moments of the cluster vary between $8\mu_B$ (Refs. 34, 41, and 43) and $27\mu_B$,[37] for Mn_7 between $5\mu_B$ (Refs. 34, 41, and 43) and $29\mu_B$,[30] for Mn_8 between $4\mu_B$ (Refs. 34 and 43) and $34\mu_B$,[36] to be compared with the experimental estimates of Knickelbein:[28] $3.3\mu_B$ for Mn_6, $5.04\mu_B$ for Mn_7, and $8.3\mu_B$ for Mn_8. The most comprehensive study for all clusters from Mn_2 to Mn_{20} has been presented by Kabir *et al.*[41] For all clusters it has been found that between two and five magnetic isomers lie in an interval of only 0.1 eV/atom above the ground state. Taking this into consideration, the variation in the magnetic moments with cluster size is in good agreement with the Stern-Gerlach experiments of Knickelbein.[28] However, the coexistence of ferromagnetic and AFM interactions suggests that the necessarily present frustration may be relieved by adopting a noncollinear magnetic configuration.

The problem of finding the correct magnetic ground state becomes even more acute if a noncollinear arrangement of the local magnetic moments is admitted. Mejia *et al.*[48] find that all clusters with $n=2\rightarrow 8$ have a noncollinear magnetic structure (although the angles between magnetic moments differ only rather little from 0° or 180°). Morisato *et al.*[47]

reported a noncollinear ground state for Mn_5 and Mn_6 clusters, Longo *et al.*[46,51] show that Mn_2 and Mn_3 clusters remain FM while clusters with 4, 5, and 6 Mn atoms adopt a noncollinear structure. For the Mn_6 cluster the magnetic structures found by Morisato *et al.* and Longo *et al.* are in reasonable agreement but those for Mn_5 are significantly different. The most complete investigation of noncollinear magnetism has again been presented by Kabir *et al.*[50] for Mn_n, $n=2-10$, 13, 15, and 19. A collinear ground state is confirmed for $n=7$, 15, and 19, for all other clusters a noncollinear structure is at least slightly lower in energy (although the canting of the directions of the local moments with respect to the global moment is sometimes rather modest). Compared to the collinear structures, total moments are sometimes reduced ($n=10$), in many cases almost unchanged ($n=8,9,13$) and in other cases even enhanced ($n=6$) compared to the collinear results. Compared to experiment agreement may be improved but also worsened. The difficulty resides in the simultaneous optimizations of all structural and magnetic degrees of freedom. Previous work on AFM Cr clusters[53] has shown that the frustration of the exchange interaction may be reduced either by geometrical distortions or by adopting a noncollinear magnetic structure (or both). Unfortunately the work of Kabir *et al.*[50] gives no information on the precise geometry of the clusters showing noncollinear magnetism, although their previous work[41] had shown that collinear magnetic isomers differ also in their geometrical structures (bond-length variations by several 0.1 Å have been reported).

In the present work we have investigated the magnetic properties in periodic Mn nanostructures ranging from one-dimensional wires over two-dimensional stripes to three-dimensional nanorods using *ab initio* density-functional techniques. Our model consists of six Mn atoms placed into a box with lateral dimensions large enough to ensure a sufficient separation between the periodic images of our nanostructures, and a variable length c in the third direction. At large values of c this corresponds to a straight monatomic chain of Mn atoms under tension. As c is gradually reduced, the structure transforms first to a zigzag chain, then to a two-dimensional stripe and finally to a three-dimensional nanorod. At each stage the geometric and magnetic structures are optimized, allowing for both collinear and noncollinear configurations. In addition for selected geometric structures incommensurate spin-spiral structures have been explored. This work extends a recent investigation of the magnetic properties of Fe and Ni nanostructures,[54] which was, however, restricted to collinear ferromagnetic structures.

II. COMPUTATIONAL SETUP

The quantum-mechanical framework of our investigations is spin-density-functional theory within the semilocal generalized-gradient approximation. We have used the Vienna *ab initio* simulation package (VASP) (Ref. 55) which performs an iterative solution of the Kohn-Sham equations for periodic boundary conditions in a plane-wave basis. The basis set contained plane waves with kinetic energies up to 337 eV. The electron-ion interaction was described by projector-augmented wave (PAW) potentials.[56,57] The PAW approach shares the computational efficiency of the pseudopotential approach but is an all-electron technique avoiding the problems related to the linearization of the core-valence exchange interaction (this is particularly important for magnetic calculations). We use the gradient-corrected exchange-correlation functional proposed by Perdew *et al.*[58] and the spin interpolation of Vosko, Wilks, and Nusair.[59] The use of the generalized-gradient approximation is essential for a correct description of the structural and magnetic ground state of both ferromagnets[60] and antiferromagnets.[61,62] The calculations have been performed in a scalar-relativistic mode, i.e., spin-orbit coupling has been neglected. This seems to be justified by two observations: (i) in a free Mn atom the orbital moment is zero because the $3d$ shell is exactly half filled. (ii) In our previous work on Mn monolayers and bilayers on Fe(001) (Ref. 14) very small orbital moments on the Mn atoms (less than $0.02\mu_B$) have been found. These orbital moments are smaller by a factor of 2–3 than the orbital moments of the substrate atoms. Brillouin-zone integrations have been performed on $1\times1\times30$ k-point set, using a modest Gaussian smearing of the eigenvalues. The criterion used for terminating the self-consistency iterations was the energy changed by less than 10^{-5} eV in succeeding iterations.

Noncollinear magnetism is described with the fully unconstrained formalism implemented in VASP by Hobbs *et al.*[53] Density-functional theory is expressed in terms of a 2×2 density matrix with elements $n^{\alpha\beta}(\mathbf{r})$. The electron density is given by the trace of the density matrix,

$$\mathrm{Tr}[n^{\alpha\beta}(\mathbf{r})] \equiv n_{\mathrm{Tr}}(\mathbf{r}) = \sum_{\alpha} n^{\alpha\alpha}(\mathbf{r}). \tag{1}$$

The total density matrix may then be defined as

$$n^{\alpha\beta}(\mathbf{r}) = [n_{\mathrm{Tr}}(\mathbf{r})\delta_{\alpha\beta} + \vec{m}(\mathbf{r})\cdot\vec{\sigma}^{\alpha\beta}]/2, \tag{2}$$

where $\vec{\sigma}$ stand for the vector of the Pauli matrices, $\vec{\sigma}=(\sigma_x,\sigma_y,\sigma_z)$ and where the spin density is defined by

$$\vec{m}(\mathbf{r}) = \sum_{\alpha\beta} n^{\alpha\beta}(\mathbf{r})\cdot\vec{\sigma}^{\alpha\beta}. \tag{3}$$

The magnetization density is obtained by multiplying the spin density by a factor $\frac{e\hbar}{mc}$.

The functional derivative of the DFT exchange-correlation functional with respect to the electron and spin density leads to the nonmagnetic scalar exchange-correlation potential,

$$v_{xc}[n^{\alpha\beta}](\mathbf{r}) = \frac{\delta E_{xc}[n^{\alpha\beta}]}{\delta n_{\mathrm{Tr}}(\mathbf{r})} = \epsilon_{xc}[n^{\alpha\beta}(\mathbf{r})] + n_{\mathrm{Tr}}(\mathbf{r})\frac{\partial\epsilon_{xc}[n^{\alpha\beta}(\mathbf{r})]}{\partial n_{\mathrm{Tr}}(\mathbf{r})} \tag{4}$$

and to the magnetic exchange-correlation field,

$$\vec{b}[n^{\alpha\beta}](\mathbf{r}) = \frac{\delta E_{xc}[n^{\alpha\beta}]}{\delta\vec{m}(\mathbf{r})} = \frac{\partial|\vec{m}(\mathbf{r})|}{\partial\vec{m}(\mathbf{r})}\frac{\delta E_{xc}[n^{\alpha\beta}]}{\delta|\vec{m}(\mathbf{r})|}$$

$$= \hat{m}(\mathbf{r})n_{\mathrm{Tr}}(\mathbf{r})\frac{\partial\epsilon_{xc}[n^{\alpha\beta}(\mathbf{r})]}{\partial|\vec{m}(\mathbf{r})|}, \tag{5}$$

where

$$\hat{m}(\mathbf{r}) = \frac{\partial|\vec{m}(\mathbf{r})|}{\partial\vec{m}(\mathbf{r})} \tag{6}$$

is the direction of the magnetization density at the point $\mathbf{r}$. Hence the potential $\vec{b}(\mathbf{r})$ is parallel to the magnetization density $\vec{m}(\mathbf{r})$ everywhere. For any detail of the implementation of noncollinear magnetism in the PAW formalism used in VASP we refer to the work of Hobbs *et al.*[53]

The boundary conditions applied to the unit cell also restrict noncollinear solutions to periodic magnetic structures. Incommensurate solutions which are not restricted by the choice of the periodic boundary conditions may be found by applying the generalized Bloch conditions introduced by Herring[63] (see also Sandratskii[64]) and implemented in VASP by Marsman.[65]

The implementation based on a vector-field description of the magnetization density allows a continuous variation in the direction of the local magnetic moment between atoms. In this respect it differs from alternative approaches to noncollinear magnetism admitting a fixed orientation of the spin-quantization axis around each atom.[66–68] An important example where a full vector-field description of magnetization is required to achieve a correct description of the ground state is the spin-spiral state in γ-Fe with a propagation vector $\vec{q}=\frac{2\pi}{a}\times(0.2,0,1)$ (Refs. 65 and 69)—all calculations based on atomic spin-quantization axes produce a spin spiral with $\vec{q}=\frac{2\pi}{a}\times(0,0,\sim 0.6)$.

Nanostructures were modeled by an ensemble of six atoms in a periodically repeated tetragonal cell with lateral dimensions along the x and y axes of 17 Å. The axis of the nanostructures (wire, stripe, or rod) was oriented along the z direction, tension or compression on the nanostructure was simulated by changing the height of the cell. Relaxation of the atomic structure was performed via a conjugate-gradient method, using the exact Hellmann-Feynman forces acting on the atoms. A straight monatomic wire was produced by restricting relaxation to changes in the z coordinates of the atoms. Two-dimensional stripes are generated by permitting relaxation in a plane passing through the axis of the wire while either imposing equal interatomic distances along z, ("xy relaxed") or allowing an independent relaxation of five atoms within the plane or in all three directions, imposing only the periodic boundary conditions fixed by the cell size. The position of the sixth atom is fixed in the center of the basis of the cell. If the atoms are constrained to remain within a plane, we observe with decreasing tension a transition from a straight to a zigzag wire, the formation of stripes based on triangular motifs and finally under compressive strain the disintegration into separated parallel wires. If relaxation in all three Cartesian directions is permitted, a transition to nanorods is observed. For comparison we also include nanorods formed by a periodic stacking of trigonal prisms or antiprisms which are not spontaneously formed upon compression of the cell. These two structures are relaxed only in a plane perpendicular to the axis while the distance between the triangular base and top is fixed by the periodic boundary conditions. The structural optimizations were assumed to be converged when all forces acting on the atoms were smaller than 0.001 eV/Å.

Local magnetic moments are calculated from the integrated local spin-polarized densities of states (DOS). Because the calculation of the local DOS is based on a projection of the plane-wave components of the eigenstates onto spherical waves within atomic spheres, the absolute values of the local moments depend slightly on the choice of the atomic radius. The same radius of 1.33 Å has been used for all sites in all configurations. Therefore, while the absolute values of the local moments are subject to a small uncertainty, the relative magnitude of the moments is reliably reproduced.

III. MANGANESE NANOSTRUCTURES

In the following we describe the results for the geometric and magnetic structures of the Mn nanostructures subject to a decreasing tension along the z axis. Table I summarizes the results for the local equilibrium configurations in one to three dimensions. In one dimension the result is rather simple. For collinear magnetic ordering we find FM and AFM solutions, with a distinct preference for the antiferromagnetic case which also allows for a shorter Mn-Mn bond length. What is not entirely expected is that even for a linear chain a noncollinear magnetic structure is preferred. In two and three dimensions the situation is much more complex because structural and magnetic relaxations are in competition—this leads to a situation where we find multiple local minima in the multidimensional configuration space spanned by all geometric and magnetic degrees of freedom.

A. Wires

We start our simulations from a 1D monatomic chain with equal interatomic distances. Minimization of the total energy with respect to the height c of the cell yields an equilibrium bond length of $d=2.35$ Å ($c=14.13$ Å) for an AFM, of $d=2.61$ Å for a FM, and of $d=2.418$ Å for a wire with a noncollinear magnetic structure. These interatomic distances are intermediate between the nearest-neighbor distances in α-Mn which vary between 2.2 and 2.75 Å (for details see Hobbs *et al.*[4] and Villars *et al.*[70]) but they are smaller than the equilibrium bond lengths in ferromagnetic or AFM dimers (for AFM Mn_2 Mejia-Lopez *et al.*[52] report $d=2.86$ Å while Kabir *et al.*[41] find $d=2.61$ Å). At equilibrium, the magnetic moments are 4.04, 3.70, and 3.78μ_B in the FM, AFM, and noncollinear phases, cf. Fig. 1 and Table I. For all magnetic configurations the interatomic distances are constant along the chain. Dimerization is energetically favorable only in very strongly stretched chains. This is related to the very weak binding of the Mn_2 dimer as reported by Tzeli *et al.*[44]

These magnetic moments are significantly larger than the local magnetic moments in the noncollinear magnetic α phase. In paramagnetic cubic α-Mn the atoms occupy four different types of crystallographically inequivalent sites, due to the tetragonal distortion associated with AFM ordering, types III and IV split into two subsets. MnI atoms occupy the corners and the center of the body-centered-cubic cells, they carry the largest magnetic moment of 2.83μ_B (absolute values). MnII atoms have a somewhat smaller magnetic mo-

TABLE I. Cell height c, shortest interatomic distances d (in Å), absolute values of local magnetic moments M_i, and Cartesian components (M_x, M_y, M_z) of the resultant magnetic moments per cell (in μ_B), and total energies (in eV/atom) for Mn nanostructures in one, two, and three dimensions at local equilibrium for different magnetic structures—FM, AFM, FI, NCL, and SS.

Structure	Magnetic configuration	c (Å)	d (Å)	$\lvert M\rvert_i$ (μ_B)	(M_x, M_y, M_z) (μ_B)	E_{tot} (eV/atom)
Wire	FM	15.66	2.61	4.04	(0,0,24.24)	−6.109
	AFM	14.13	2.35	3.70	(0,0,0)	−6.175
	NCL	14.46	2.42	3.78	(0,−3.73,0.15)	−6.230
	SS[a]	14.46	2.42	3.79	(0,0,0)	−6.229
Triangular stripe	FM	8.10	2.56	3.85	(0,0,23.10)	−6.739
	AFM1	7.92	2.50	3.71	(0,0,0)	−6.706
	AFM2	7.44	2.40	3.38,3.87	(0,0,0)	−6.839
	NCL1(Néel)	7.38	2.46	3.63	(0,−4.76,−1.73)	−6.772
	NCL2(3Q)	7.34	2.44	3.48,3.69	(0,0,0)	−6.832
	SS[a]	7.38	2.46	3.63		−6.783
Hexagonal stripe	FM	5.34	2.56	3.59,3.90	(0,0,22.78)	−6.835
	AFM1	5.34	2.33	2.71,3.68	(0,0,0)	−7.002
	AFM2	4.99	2.41	3.37,3.63	(0,0,0)	−7.058
	FI1	5.04	2.46	3.00,3.31,3.48,3.79	(0,0,0.93)	−7.069
	FI2	5.19	2.33	2.82,3.48,3.90	(0,0,−6.49)	−7.099
	NCL1(Néel)	5.06	2.53	3.41,3.71	(0.42,−0.27,−0.11)	−7.058
	NCL2(3Q)	5.18	2.36	3.23,3.57,3.70	(0,2.2,−2.73)	−7.074
	SS[a]	5.06	2.53	3.29,3.75		−7.042
Prismatic rod	AFM1	4.803	2.40	3.64	(0,0,0)	−6.942
	AFM2	4.781	2.39	3.34,3.49	(0,0,0)	−7.061
Tetrahedral rod	AFM	5.093	2.28	3.31,3.55	(0,0,0)	−7.184
	NCL	5.029	2.32	3.40,3.51	(0,0.01,0.04)	−7.214
Octahedral rod	AFM	3.689	2.38	1.18,3.50	(0,0,0)	−7.503
	NCL	3.581	2.34	1.88,3.50	(−0.71,−7.15,−0.02)	−7.509

[a]Calculations for spin spirals have been performed at a fixed geometry identical to that of the NCL (NCL1) phases.

ment of $1.83\mu_B$ while MnIIIa and MnIIIb carry magnetic moments of 0.74 and $0.48\mu_B$, and MnIVa and MnIVb atoms have moments of 0.59 and $0.66\mu_B$ according to the magnetic neutron-diffraction data of Lawson *et al.*[5] The DFT calculations have elucidated the mechanism leading to the formation of a noncollinear magnetic structure; under compression, the MnIV atoms forming a triangular arrangement become nonmagnetic and simultaneously the noncollinearity vanishes, in an expanded state the MnIV moments increase and the canting of all magnetic moments becomes more pronounced. Hence noncollinearity arises from the frustration of the AFM interaction between the MnIV atoms occupying triangular motifs with short interatomic distances and is essentially the result of a geometric frustration.

It is therefore quite surprising that in a Mn nanowire the magnetic ground state is also noncollinear, with an energy which is 55 meV/atom lower than in the collinear AFM state. The noncollinear magnetic structure of the wire is similar to that of the noncollinear Néel phase of a frustrated triangular antiferromagnet.[21] Spins on neighboring sites are rotated by 120°, in addition they are slightly canted relative to the plane in which they are rotated (see Fig. 1), resulting in a net magnetic moment nearly perpendicular to the wire.

The three different magnetic configurations display strongly contrasting electronic structures. Figure 2 shows the spin-polarized local electronic DOS at a Mn atom of the monowire in the FM, AFM, and noncollinear states. An AFM wire is characterized by a narrow, strongly exchange-split d band. The band of the occupied majority states is centered at an energy −2.80 eV below the Fermi energy, the bandwidth of the d_{xy} and $d_{x^2-y^2}$ components forming $dd\delta$ bands is less than 0.5 eV, the majority $dd\pi$ band formed by the d_{xz} and d_{yz} states is only slightly broader. The d_{z^2} states form $dd\sigma$ bonds and hybridize with the s states through $ds\sigma$ matrix elements. As a consequence they undergo a stronger broadening. The minority-spin states are more extended, leading to a more pronounced broadening of the d_{xz} and d_{yz} states, the lower edge of the band overlapping with the Fermi level. The $dd\delta$ bands are completely spin-polarized, spin polarization is weaker for the $dd\pi$ band and almost absent for the $dd\sigma$ band—this explains the magnetic moment of $3.70\mu_B$. It is remarkable that the ratio of exchange splitting ($\Delta_{ex} \sim 3.8$ eV) and of the local magnetic moment ($M=3.70\mu_B$) corresponds to a value of the Stoner parameter $I=\Delta_{ex}/M$ of

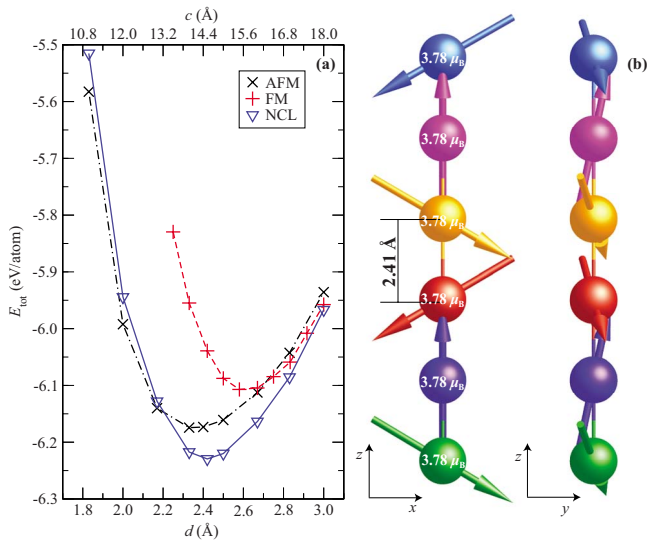

FIG. 1. (Color online) (a) Energy vs interatomic distance for FM, AFM, and noncollinear magnetic wires of Mn atoms and (b) equilibrium noncollinear magnetic structure of a straight Mn monowire. Cf. text.

$I \sim 0.97$ eV/μ_B very close to the universal value of $I \sim 0.95 \pm 0.1$ eV/μ_B for bulk itinerant ferromagnets and antiferromagnets.[71–73]

In contrast, the bands of a FM Mn monowire are much wider, they show the characteristic structure of a 1D chain of d-metal atoms with a narrow $dd\delta$ (d_{xy} and $d_{x^2-y^2}$) band, a somewhat wider $dd\pi$ (d_{xz} and d_{yz}) band, and a very broad $dd\sigma$ (d_{z^2}) band, all displaying the DOS maxima at the band-edges characteristic for a one-dimensional configuration. The differences in the degree of spin polarization are less pronounced than for the AFM configuration. The exchange splitting is different for the three subbands, it is largest for the δ component (about 4.1 eV) and smallest for the π-bonded states (about 3.2 eV), in accordance with the degree of spin polarization. On average, an exchange splitting of $\Delta_{ex} \sim 3.5$ eV and a magnetic moment of $4.04\mu_B$ leads to a value of the Stoner parameter close to that calculated for the AFM phase. For the noncollinear phase no decomposition of the total DOS into majority and minority components is possible (only for the local atomic DOS an approximate decomposition with respect to a quantization axis oriented along the direction of the average local moment would be possible). The total spin-averaged DOS [see Fig. 2(c)] shows a character intermediate between the ferromagnetic and AFM solutions: very narrow and completely spin-polarized $dd\delta$ band, bandwidth and degree of spin polarization decreasing in the sequence $dd\delta \rightarrow dd\pi \rightarrow dd\sigma$. The differences in the exchange splitting between the subbands is slightly larger but leads again to the same universal value of the Stoner parameter. The sum of the one-electron energies is lower for the noncollinear than for the antiferromagnetic and FM configurations.

The AFM, FM, and "Néel" phases of the Mn wire may be regarded as special cases of a spin spiral (SS). The stability of the different magnetic configurations may be discussed in terms of a simple Heisenberg model (forgetting for the moment that the Mn nanostructures are itinerant magnets). For a strictly periodic chain, the rotation of the magnetic moment from one site to the next must be constant along the chain. Hence with exchange-pair interactions J_n between nth nearest neighbors the total energy is given by

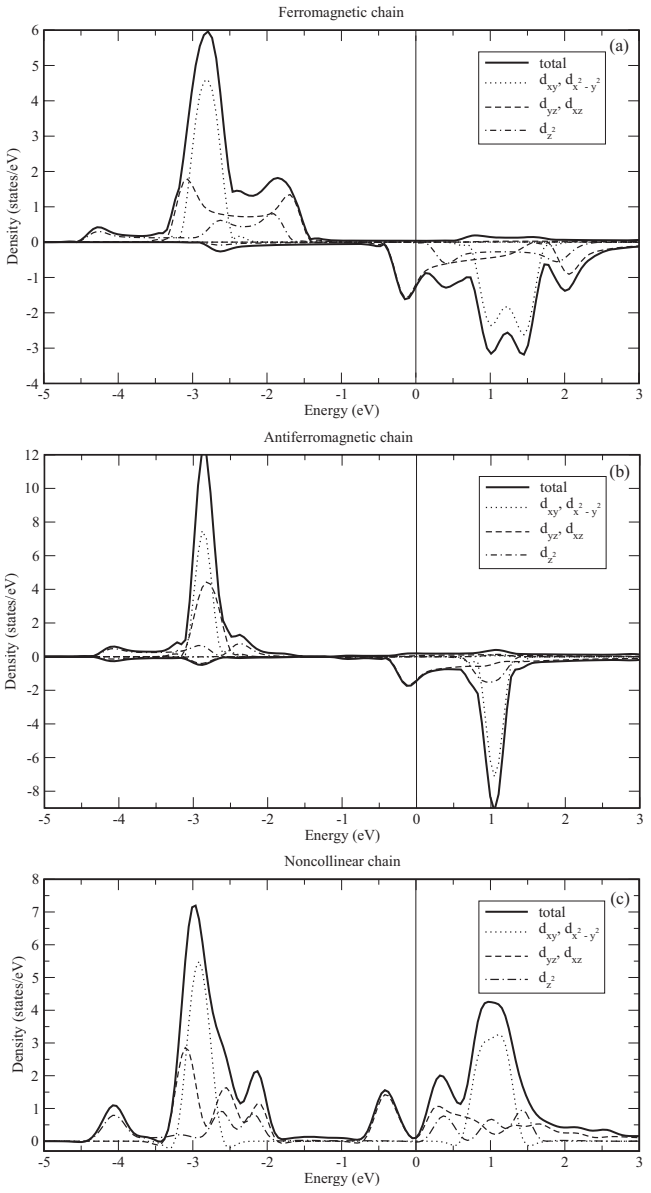

FIG. 2. Electronic density of states of a straight Mn monowire: [(a) and (b)] spin-polarized local and angular momentum decomposed density of states at a Mn atom in (a) a FM and (b) an AFM wire. (c) Total and angular-momentum decomposed density of states of a wire with a noncollinear magnetic structure. Cf. text.

$$E = 2J_1 \cos\phi - 2J_2 \cos 2\phi + 2J_3 \cos 3\phi \ldots . \qquad (7)$$

If the range of the exchange interaction is restricted to nearest and next-nearest neighbors, the extrema of the total energy with respect to variations in the angle of rotation are determined by the condition

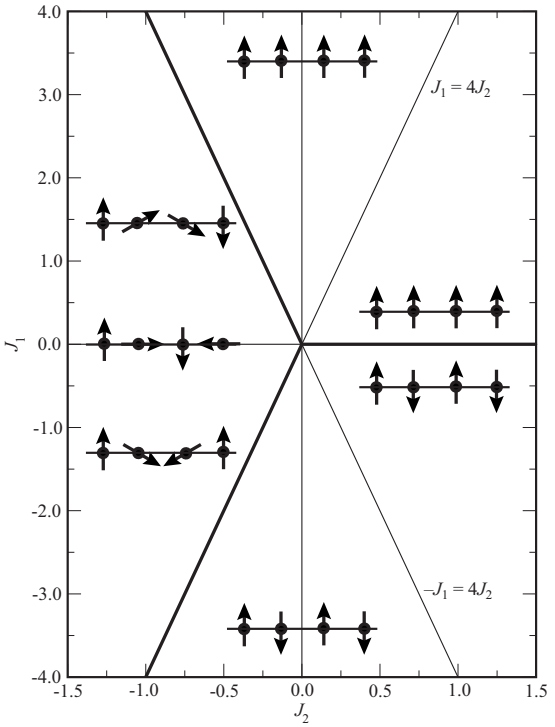

FIG. 3. Phase diagram of a Heisenberg model of a straight magnetic wire with nearest (J_1) and next-nearest (J_2) exchange interactions. Cf. text.

$$\frac{\partial E}{\partial \phi} = 2 \sin \phi (J_1 + 4J_2 \cos \phi) = 0. \tag{8}$$

This condition has multiple solutions: (i) $\sin \phi = 0$ describing the FM ($\phi = 0°$) and AFM ($\phi = 180°$) solutions, and (ii) $\cos \phi = -\frac{J_1}{4J_2}$ describing a spin spiral. For $|\frac{J_1}{4J_2}| \geq 1$ only the collinear solutions exist. Outside this range, the collinear solutions are lower in energy than the noncollinear spin-wave state for $J_1 \geq 0$ whereas the spin-wave solutions are preferred for $J_1 \leq 0$. A Néel phase with an angle of rotation of 120° is stabilized for J_1, $J_2 \leq 0$, and $J_1 = 2J_2$. The spin-wave solutions are twofold degenerate for clockwise and anticlockwise rotations of the spins. A schematic phase diagram for the Heisenberg chain is shown in Fig. 3. The noncollinear phase with an angle of rotation of about 120° is found to arise from strong AFM interactions between both nearest and next-nearest neighbors. Hence in contrast to the bulk phases, the frustration arises from the competition between short-range and long-range AFM coupling.

Periodic boundary conditions suppress incommensurate spin waves. Hence the solution with $\phi = 120°$ resulting from the DFT calculations could be imposed by the periodicity of the computational cell (six times the interatomic distance) while the sign and relative magnitude of nearest-neighbor and next-nearest-neighbor exchange interactions would prefer a different angle of rotation between nearest-neighbor spins. An incommensurate solution which is not restricted by the choice of the periodic boundary conditions may be found by applying the generalized Bloch conditions introduced by Herring[63] and implemented in VASP by Marsman.[65] Figure 4

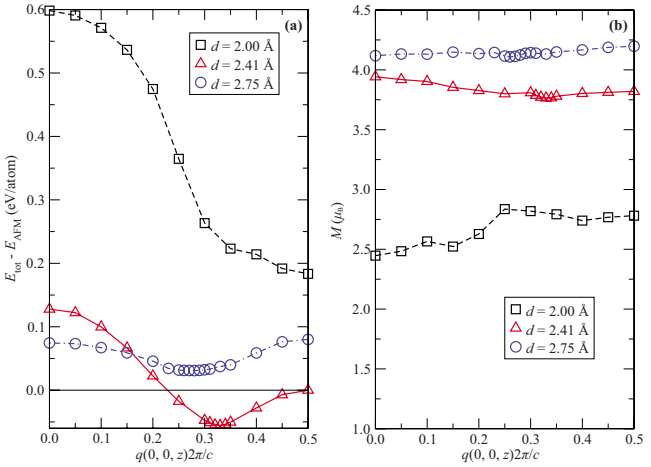

FIG. 4. (Color online) (a) Total energy relative to the AFM state and (b) magnetic moments of an incommensurate spin spiral on a Mn chain, calculated as a function of the spiral wave vector and for different interatomic distances. Cf. text.

shows the total energy and magnetic moments of a SS on a periodic Mn wire as a function of the wave vector, calculated for different interatomic distances. At the equilibrium distance ($d = 2.41$ Å) calculated for the noncollinear periodic phase, we find a minimum for a SS with $\vec{q} = (0,0,0.33) \times \frac{2\pi}{c}$ which coincides with the periodic noncollinear solution. The FM state at the zone center and the AFM state realized at $\vec{q} = (0,0,0.5) \times \frac{2\pi}{c}$ are higher in energy. Remarkably, the magnetic moment is almost independent of the wave vector of the SS, as a consequence of the large exchange splitting—this justifies our simple Heisenberg model. If the Mn chain is expanded to $d = 2.75$ Å, the FM state becomes favored over the AFM state but the energetically most favorable solution is an incommensurate SS with $\vec{q} \sim (0,0,0.28) \times \frac{2\pi}{c}$. If the chain is compressed (while maintaining the strictly one-dimensional structure), the total energy of the FM and SS solutions increase strongly relative to the AFM solution, the spin-spiral solution becomes unstable. With the simple Heisenberg model discussed above, this corresponds to an increase in the nearest-neighbor exchange coupling such that $|J_1| \geq |4J_2|$.

B. From wires to stripes

When the height of the computational cell is reduced the straight wire adopts a zigzag structure which transforms upon decreasing tension first to a triangular and then to a hexagonal stripe. The relaxation of the atomic coordinates has been performed in two different modes: keeping the atoms equidistant along the z direction (xy relaxed) or allowing an unconstrained relaxation. The constrained relaxation leads to a gradual transformation from a straight to a zigzag wire and further to a triangular stripe while maintaining the same type of noncollinear magnetic structure as shown in Fig. 5(a). An unconstrained relaxation leads to a different scenario for the transformation from a one-dimensional nanostructure to a two-dimensional nanostructure, even at a modest reduction in the cell height the formation of

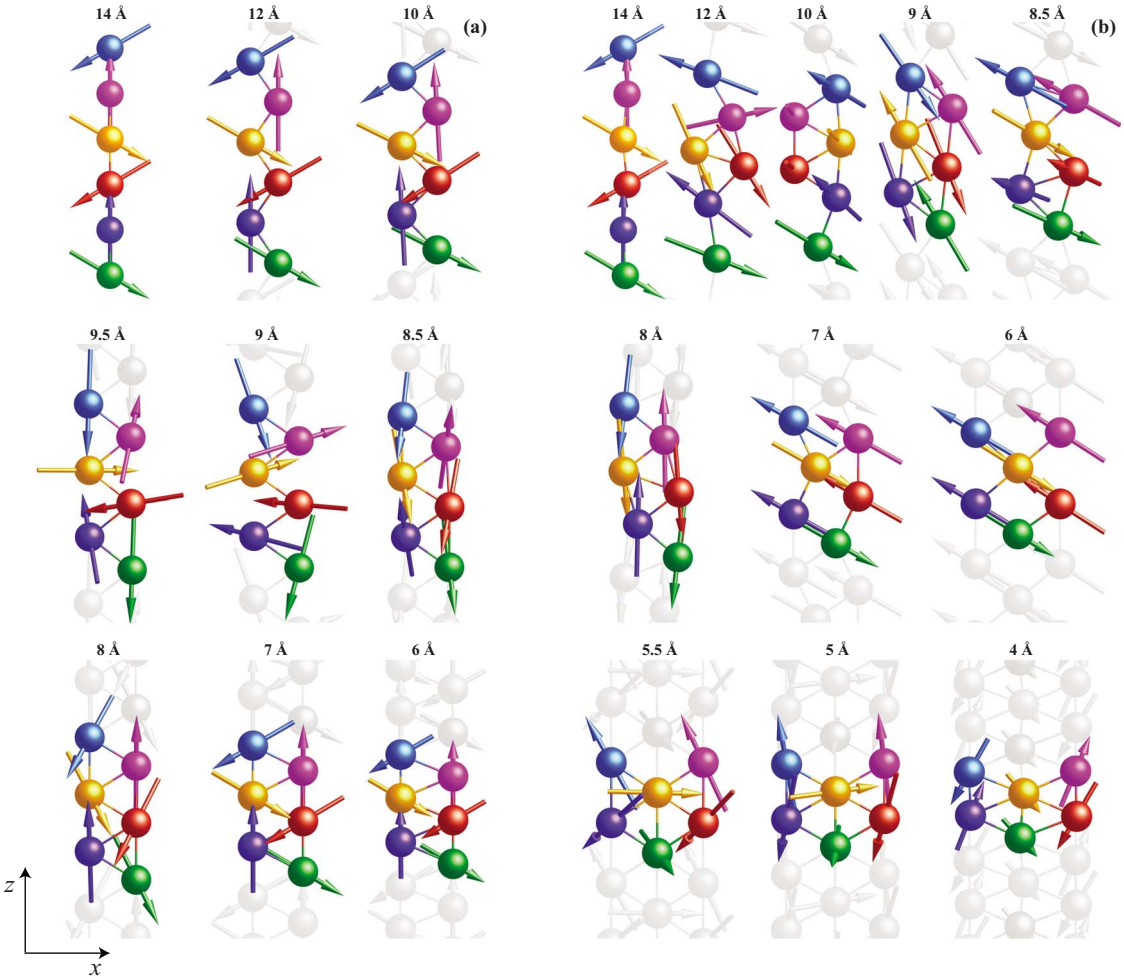

FIG. 5. (Color online) Geometric and magnetic structures of one- and two-dimensional Mn nanostructures for varying height of the computational cell, (a) produced by *xy* relaxation where the difference in the *z* coordinates of neighboring atoms is the same for all atoms and (b) resulting from an unconstrained relaxation in a plane. Cf. Fig. 6 and text.

crosslinks between atoms favors clustering in the center of the cell while some of the outer bonds are broken, see Fig. 5(b). In this case no continuous triangular stripe is formed. At a cell height of $c \sim 8$ Å corresponding to the local equilibrium for a triangular stripe [see Fig. 6(a)] a cluster with a similar geometry but contracted interatomic distances is formed. The change in the geometric structures is also reflected in the magnetic structures. In a zigzag chain where all

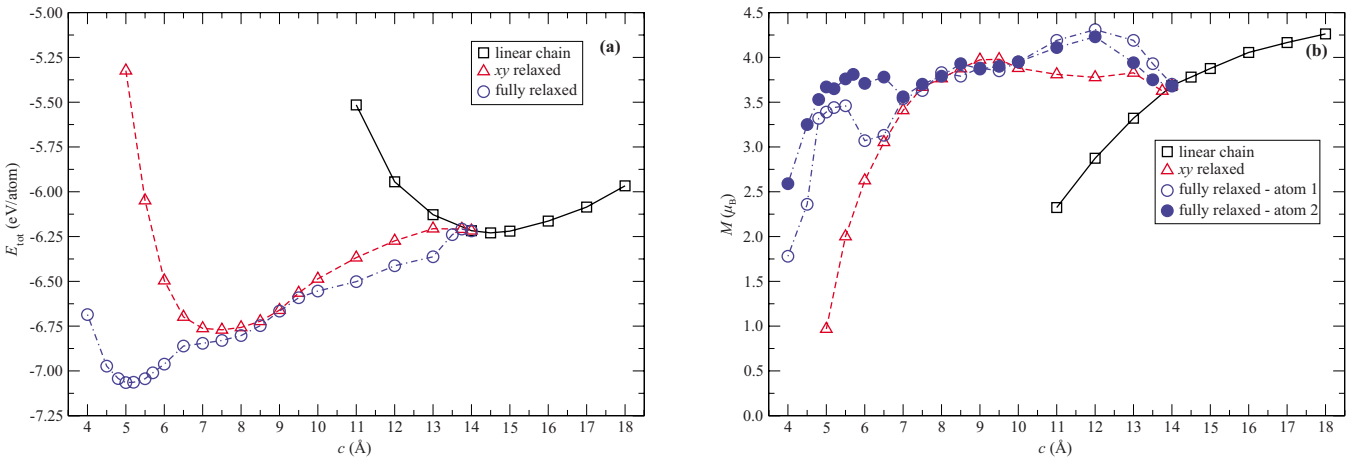

FIG. 6. (Color online) (a) Total energy and (b) magnetic moments (per Mn atom) of one- and two-dimensional Mn nanostructures as a function of varying height of the computational cell. Cf. Fig. 5 and text.

interatomic distances are equal the Néel structure remains energetically favorable down to $c \sim 10$ Å. At this point the magnetic moments begin to rotate, at $c \sim 9.5$ Å the magnetic structure consists of pairs of antiferromagnetically coupled spins, with the pair located at the two central atoms roughly perpendicular to the spins on the outer atoms. At $c \sim 8.5$ Å the moments are aligned roughly parallel to the edges of the stripe. The periodicity does not allow to form an AFM sequence but imposes an $\ldots\downarrow\uparrow\downarrow\downarrow\uparrow\downarrow\ldots$ alternation such that the AFM coupling is necessarily frustrated. Upon further compression of the stripe, a Néel structure with 120° angles between neighboring moments and alternating positive and negative helicities of the triangles is adopted. This structure is conserved over a wide range of further compression, although the magnitude of the moments decreases [see Figs. 5(a) and 6(b)]. For the structures produced by unconstrained relaxation we note a tendency to stabilize collinear or nearly collinear magnetic structures which is most pronounced at $c \sim 9 \rightarrow 6$ Å [see Fig. 5(b)]. This reflects the fact that in the absence of geometric constraints, frustrations of the magnetic interaction may in many cases be relieved by structural distortions. Upon further compression to $c \sim 5.5$ to 4 Å complex three-dimensional noncollinear magnetic structures are adopted.

Figure 6(b) shows the variation in the magnetic moments in the one- and two-dimensional nanostructures as a function of the cell height (measuring the average interatomic distance). While for a straight wire the magnetization varies roughly as $M \propto |d-d_c|^{\beta}$ with $\beta \sim 0.5$ and $d_c \sim 1.35$ Å (corresponding to a second-order transition with mean-field exponents), for the two-dimensional stripes the magnetization decreases rather abruptly once the interatomic distances fall below a critical value.

It must be emphasized, however, that the geometric and magnetic structures shown in these graphs are generated by a stepwise contraction of the nanostructures along the z axis and do not necessarily represent the ground state which may not be reached in this way. A more detailed exploration of the magnetic configuration space has been performed around the local equilibria for triangular and hexagonal stripes.

C. Stripes

Figure 6 shows the variation in the total energy of Mn wires and stripes as a function of the height of the computational cell, as resulting from a step-by-step compression of a straight wire under different constraints. In the following we discuss the local equilibrium configurations found with the two different relaxation modes, based on a more extended search in geometric and magnetic configuration space (using different initializations for the geometric and magnetic structures).

1. Triangular stripes

If a collinear magnetic structure is assumed, xy relaxation leads to local equilibria for a FM triangular stripe with magnetic moments of $3.85\mu_B$ at $c=8.10$ Å which is about 33 meV/atom lower in energy than the configuration AFM1 at $c=7.92$ Å, consisting of a stripe of isosceles triangles [see Figs. 7(a) and 7(b)]. Equilibrium cell heights and interatomic distances have been determined by a smooth interpolation between the data points shown in the figure. All Mn atoms have a magnetic moment of $\pm 3.71\mu_B$, atoms along the edges of the stripe are ferromagnetically coupled, coupling across the stripe is AFM. The distance between antiferromagnetically coupled atoms is slightly shorter ($d=2.50$ Å) than between ferromagnetically coupled pairs ($d=2.64$ Å). This solution corresponds essentially to the rowwise 2×1 AFM state which is the ground state of a free-standing triangular Mn layer if the spin orientation is restricted to the atomic plane.[22,23] However, this is not the AFM configuration with the lowest energy.

If a noncollinear spin structure is admitted the resulting equilibrium configuration depends on the initial magnetic structure. If the calculation is started from a planar Néel structure with magnetic moments on neighboring sites rotated by 120° and alternating positive and negative helicity in the triangles forming the stripe, the system relaxes to a local equilibrium at $c=7.38$ Å and a total-energy lower by 33 meV/atom than in the FM state [configuration NCL1, see Fig. 7(d)]. Interatomic distances along the stripe are 2.46 Å, distances across the strip are 2.57 Å and the acute angle in the isoceles triangle is 57°. All atoms have a magnetic moment of $3.63\mu_B$, projected on x and z planes, the angle between neighboring moments remains close to 120° such that the frustration of the AFM nearest-neighbor coupling in the triangles is relieved. The relative orientation of next-nearest-neighbor moments is FM. However, the moments are rotated out of the plane [see Fig. 7(d)], and this leads to an appreciable net magnetic moment so that this configuration can be described as noncollinear FI.

If the magnetic structure is initialized with substantial components of the moments perpendicular to the plane of the stripe [essentially in a configuration corresponding to the "3Q" structure described by Kurz *et al.*[23] for Mn/Cu(111) monolayers], the stripe is contracted ($c=7.34$ Å) and the total energy is further reduced by 60 meV/atom. The geometric and magnetic structure of configuration NCL2 is shown in Fig. 7(e). The distortion of the triangles is stronger than in the configuration NCL1, interatomic distances vary between 2.44 and 2.62 Å. The magnetic moment of the atom occupying the acute angle (55.7°) is slightly larger ($3.69\mu_B$) than that on the other two sites ($3.48\mu_B$). The magnetic structure of the stripe may be considered essentially as consisting of two commensurate spin spirals running along the edges of the stripe, similar to the noncollinear structure found for the one-dimensional wire. The two SS are coupled antiferromagnetically across the stripe such that the lower magnetic moments couple in pairs across the short diagonal of a parallelogram whereas the larger moments couple antiferromagnetically through the long diagonal. The difference between configurations NCL1 and NCL2 is in the coupling between next-nearest neighbors. In a parallelogram formed by two edge-sharing triangles, in the state NCL1 the spin coupling is under 120° along the edges and the short diagonal and FM along the long diagonal. In state NCL2 the coupling is ~120° along the edges and AFM along the short and long diagonals. In this configuration the total magnetic moment is exactly zero, hence NCL2 is a noncollinear AFM phase.

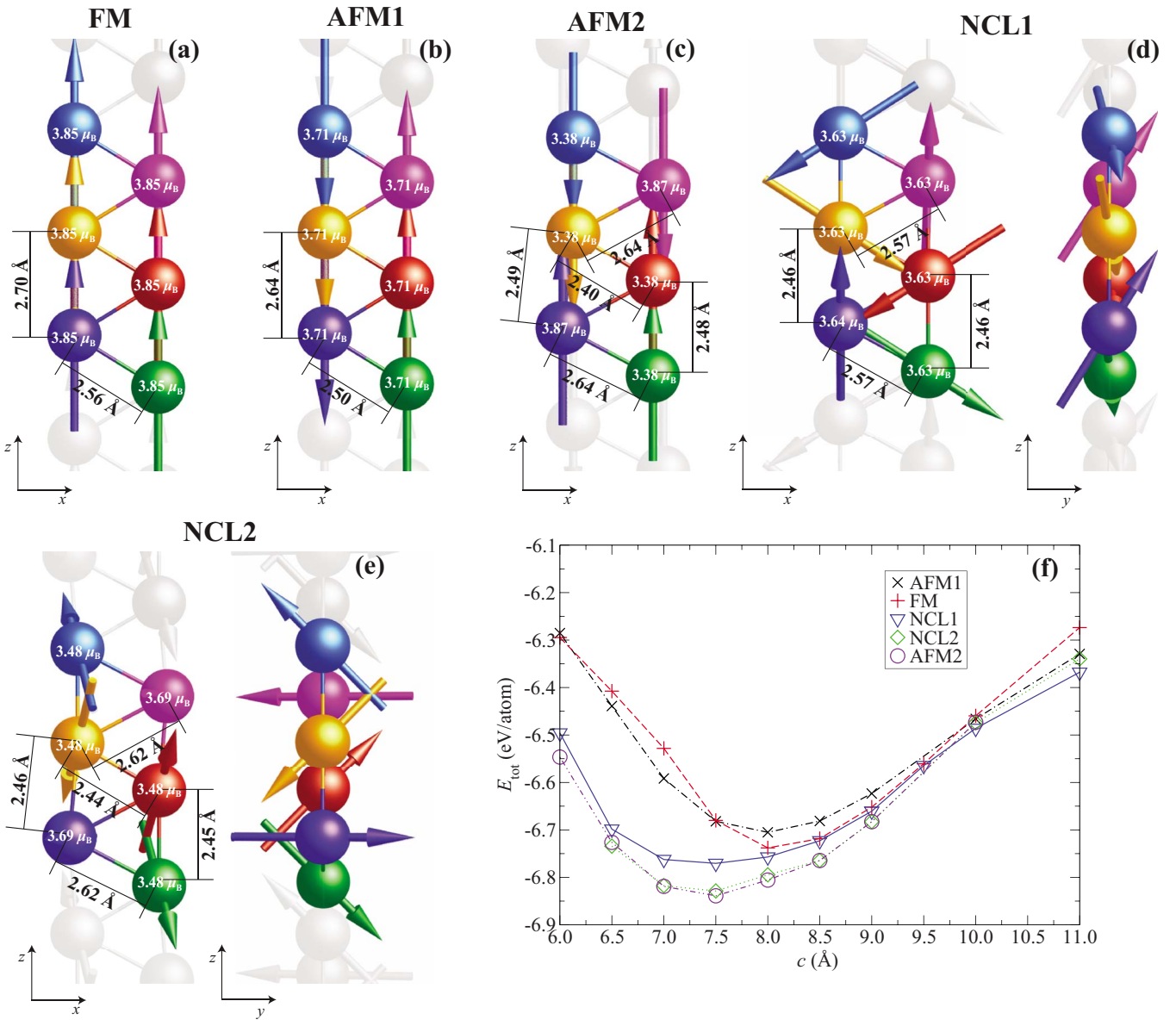

FIG. 7. (Color online) Geometric and magnetic structures of a flat triangular stripe of Mn atoms in different locally stable magnetic configurations: (a) FM, [(b) and (c)] antiferromagnetic (AFM1 and AFM2), and [(d) and (e)] noncollinear (NCL1 and NCL2). The configuration NCL1 is derived from a planar Néel-type starting configuration and is ferrimagnetic, configuration NCL2 is derived from a 3Q starting configuration and is AFM. Part (f) shows the energies of all configurations as a function of the cell height. Cf. text.

Configuration NCL2 is energetically almost degenerate with a collinear configuration AFM2 which is related to an even stronger distortion of the triangular geometry and larger differences in the local magnetic moments [3.87 and 3.38μ_B, see Fig. 7(c)]. This configuration consists of isosceles triangles with edges of 2.40 and 2.64 Å of ferromagnetically aligned moments, two such triangles couple antiferromagnetically along bonds of 2.49 Å.

The electronic densities of states of the collinear magnetic phases of the stripe are compared in Fig. 8. The FM phase has a very simple two-peaked DOS with a pronounced bonding-antibonding splitting in the majority band and a broader, less structured minority band. In contrast to the one-dimensional Mn wires, the bandwidth of the AFM stripes is not significantly reduced as compared to the FM phase because in both configurations we have FM coupling in part of the stripe: along the edges for AFM1 and in triangles for AFM2. A striking feature is that the DOS of the minority states is strongly structured for the energetically favored AFM2 and noncollinear NCL2 configurations, with a deep DOS minimum at the Fermi level. Inspection of the partial DOS shows that for configuration AFM2 the occupied minority states are mostly d_{xz} and d_{yz} states promoting bonds between the ferromagnetically coupled atoms across the stripe which are longer than the bonds along the edges. A similar statement also applies to the most favorable noncollinear state NCL2 [see also Figs. 7(c) and 7(e)].

We have also investigated the formation of spin spiral with a wave vector oriented along the direction of the stripe. The geometric structure is the same as the equilibrium struc-

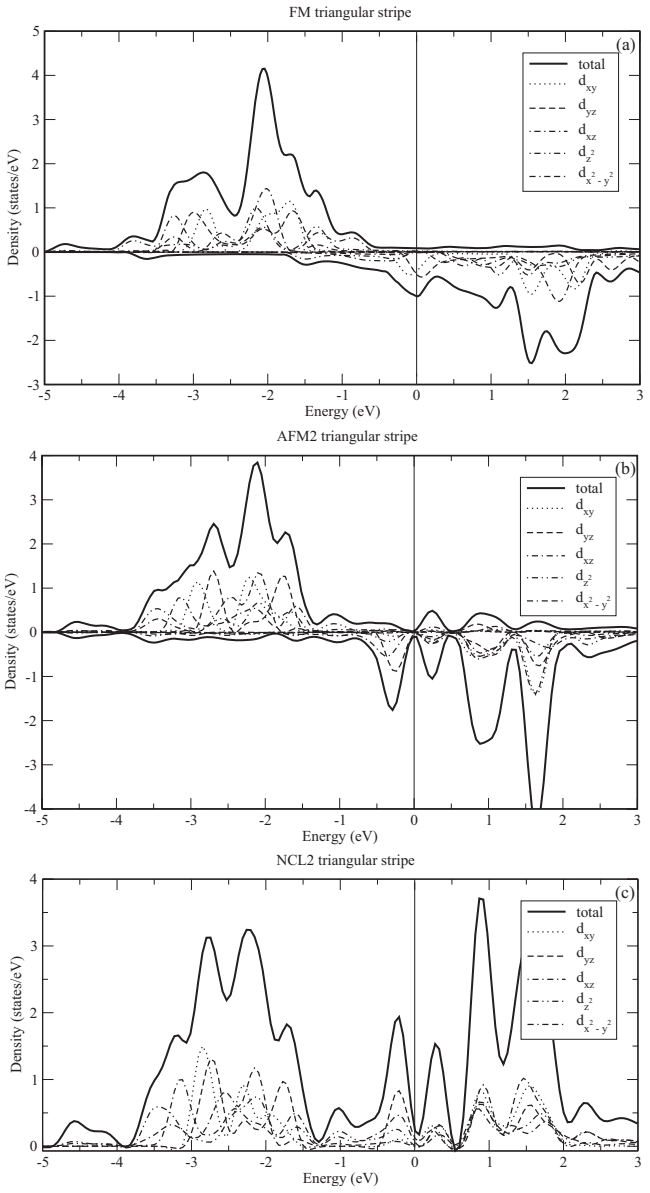

FIG. 8. Electronic density of states of a triangular stripe of Mn atoms: [(a) and (b)] spin-polarized local and angular momentum decomposed DOS of the collinear ferromagnetic and antiferromagnetic (AFM2) phases and (c) total and angular momentum decomposed DOS of the noncollinear AFM configuration NCL2. Cf. text.

ture of configuration NCL1 with straight Mn wires along the edges. The primitive unit cell for this configuration contains two inequivalent sites, for $q=0$ the magnetic moments at these sites can be either parallel or antiparallel. For larger wave vectors both solution converge to the same result. The equilibrium configuration is an incommensurate spin spiral with $\vec{q}=(0,0,0.4)\times\frac{2\pi}{c}$, corresponding to a rotation of the magnetic moment by 72° from atom to atom (see Fig. 9). The total energy is −6.783 eV/atom, i.e., 56 meV above the AFM2 state but slightly lower than for configuration NCL1 (see Table I). Since the geometric structure supporting the SS has been frozen, a lower energy could eventually be found for a fully relaxed incommensurate spin spiral. The geometric relaxation would have to be performed separately for any

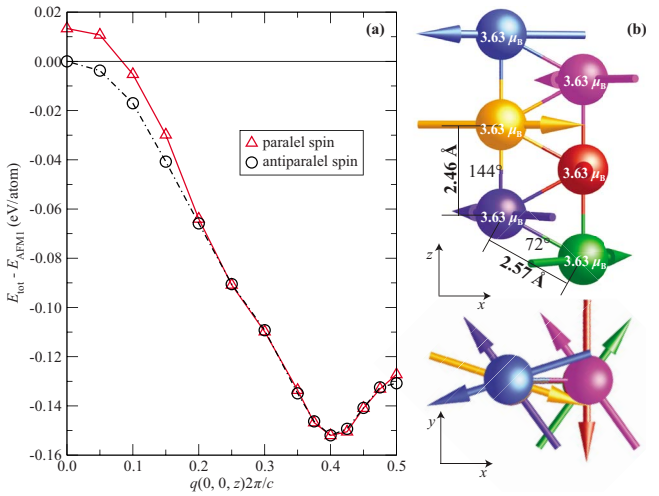

FIG. 9. (Color online) (a) Relative energy as a function of the wave vector. (b) Geometric and magnetic structures of a spin spiral formed on a flat triangular stripe of Mn atoms (fixed geometry). Cf. text.

value of the wave vector. This would require a very large computational effort. It remains an open question whether this would eventually lead to a new minimum-energy configuration.

2. Hexagonal stripes

Unconstrained relaxation within a plane leads to the formation of a broader stripe consisting of a distorted hexagonal arrangement of the Mn atoms and a noncollinear magnetic structure (see Figs. 5 and 6). Again we have performed a more extensive search for low-energy structures around the energy minimum, using different initializations of the geometric and magnetic structures. For the hexagonal stripes we have found local minima corresponding to a collinear FM state, two collinear antiferromagnetic states AFM1 and AFM2 with small differences in the atomic geometry and the magnetic moments, two collinear FI configurations FI1 and FI2 with widely different net magnetic moments per cell, and two noncollinear AFM configurations NCL1 (starting from a flat Néel structure) and NCL2 (starting from a three-dimensional 3Q structure). The lowest energy is found for the configuration FI2, it is lower in energy by 41 meV/atom than the configuration NCL1 resulting from a step-by-step compression starting from a one-dimensional nanostructure. Geometric data and magnetic moments are summarized in Table I and Fig. 10.

The antiferromagnetic configuration AFM1 at $c=5.34$ Å consists of two dimerized FM chains of opposite magnetic moments ($M=\pm 3.68\mu_B$) at the edges of the stripe and an AFM chain with lower magnetic moments ($M=\pm 2.71\mu_B$) in the center. The AFM chain has a zigzag structure because the distances between antiferromagnetically coupled pairs ($d=2.33$ Å) of atoms are smaller than between ferromagnetically aligned moments ($d=2.48$ Å). Both distances are significantly lower than between the atoms occupying the FM chains at the edges ($d=2.61$ Å and $d=2.72$ Å). The configuration AFM2 at $c=4.99$ Å consists of three parallel

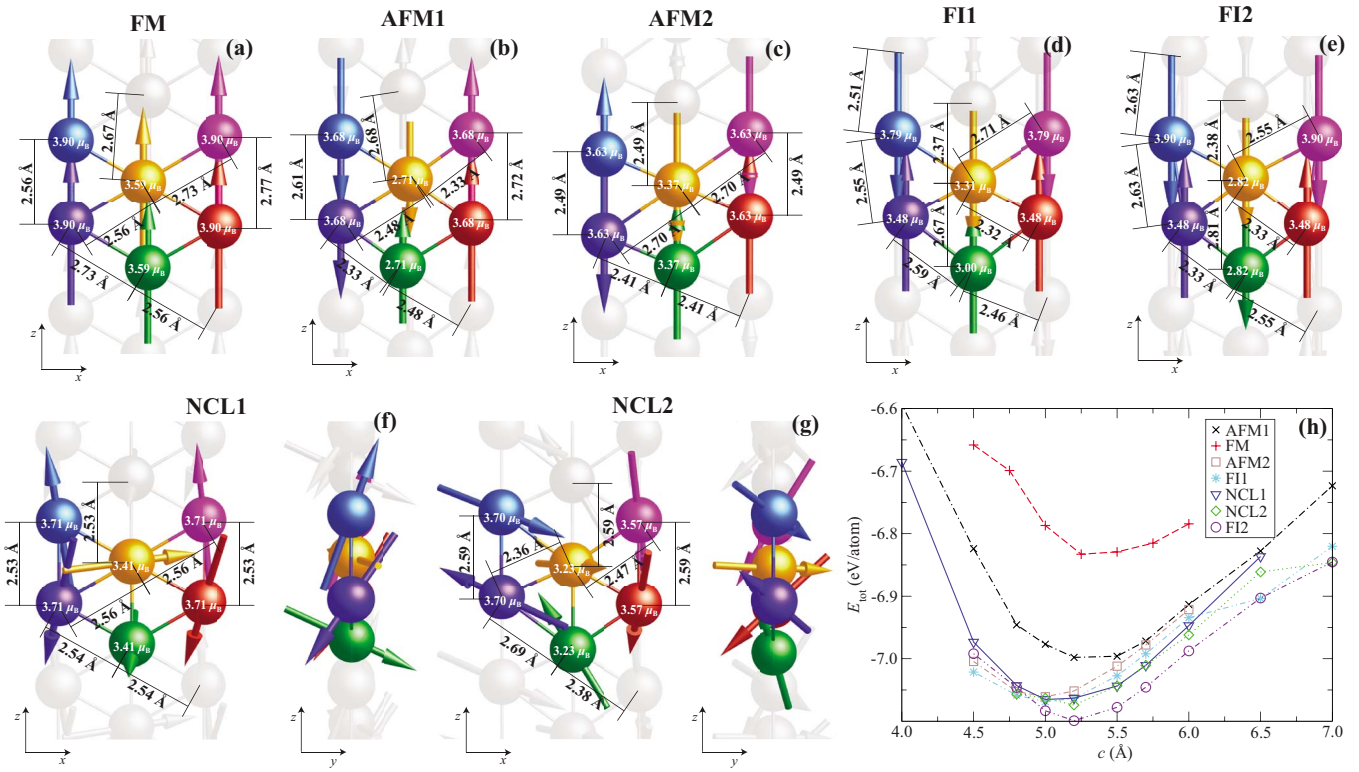

FIG. 10. (Color online) (a) Geometric and magnetic structures of a flat hexagonal stripe of Mn atoms in a ferromagnetic state, [(b) and (c)] in two locally stable collinear AFM states, [(d) and (e)] in two locally stable collinear FI states, and [(f) and (g)] in two locally stable noncollinear structures. The calculations leading to the noncollinear structures have been initialized with a planar Néel structure and a three-dimensional 3Q magnetic structure, respectively. The total energy of all configurations as a function of cell height is shown in part (h). Cf. text.

AFM chains with constant interatomic distances of 2.49 Å, the magnetic moments at the edges of the stripe ($M=\pm 3.63\mu_B$) are larger than those on the central chain ($M=\pm 3.37\mu_B$). The hexagonal arrangement of the atoms is sheared parallel to the axis of the stripe, the mechanism leading to this shear distortion is again the tendency to enhance the distances between ferromagnetically aligned moments ($d=2.70$ Å) and to shrink the distance in antiferromagnetically aligned pairs ($d=2.41$ Å). The average of long and short distances across the stripe is close to the interatomic distance along its axis.

The ferrimagnetic configuration FI1 at $c=5.04$ Å consists of a similar arrangement of three stripes with alternating positive and negative magnetic moments but because the moments have different magnitude ($\Delta|M_i|=0.31\mu_B$) the chains are FI, the net moment per cell is $0.93\mu_B$. All three chains are dimerized but the difference between long and short distances is larger for the central chain ($\Delta d=0.30$ Å) than along the edges ($\Delta d=0.04$ Å). The chains at the edges adopt a zigzag structure, again because of different nearest-neighbor distances in ferromagnetically and antiferromagnetically coupled pairs. This FI configuration is lower in energy by 11 and 67 meV/atom than the antiferromagnetic configurations AFM2 and AFM1, respectively, but lies in energy in between two noncollinear configurations (see below). A second ferrimagnetic configuration FI2 can be produced at the expense of an even stronger geometric distortion. It consists of two dimerized zigzag FI chains at the edges with alternating large negative ($-3.90\mu_B$) and small positive ($+3.48\mu_B$) moments and an even more strongly dimerized straight FM chain with moments of $2.82\mu_B$ in the center [see Fig. 10(e)]. All local magnetic moments add to a net large magnetic moment oriented in the z direction. Configuration FI2 is lower in energy by 30 meV/atom than FI1 and represents the ground state of a hexagonal stripe.

Calculations admitting a noncollinear structure have been initialized with a planar Néel and a three-dimensional 3Q-type structure, respectively, and result in configurations NCL1 and NCL2. This last calculation leads to a lower energy which is, however, still higher by 25 meV than for the FI2 state. In this configuration the atoms are aligned antiferromagnetically with moments of $3.70\mu_B$ along one edge and almost antiferromagnetically with moments of $3.57\mu_B$ along the other edge. Atoms in the center of the stripe carry lower moments of $3.23\mu_B$ [see Fig. 10(g)]. However, the moments are strongly misaligned, with a net magnetic moment of $|M_{tot}|=3.50\mu_B$ per cell. If the magnetic moments are initialized in a planar Néel configuration, relaxation leads to a rotation of the magnetic moment out of the plane formed by the atoms while the projections of the moments on the plane do not deviate too far from the Néel model [see Fig. 10(f)]. The magnetic moments are $3.41\mu_B$ in the center and $3.71\mu_B$ along the edges of the stripe, the geometric structure consists of nearly equilateral triangles with edges of 2.54 ± 0.01 Å. In this case the stability of a true Néel structure is suppressed by the periodic boundary conditions; the formation of spin

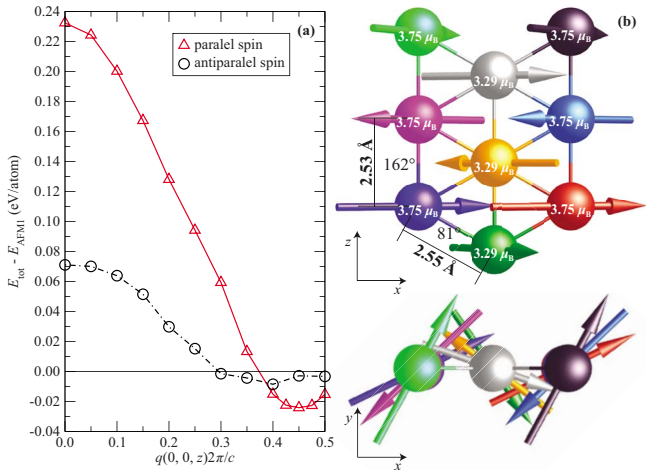

FIG. 11. (Color online) (a) Relative energy as a function of the wave vector. (b) Geometric and magnetic structures of a spin spiral formed on a flat hexagonal stripe of Mn atoms (fixed geometry). Cf. text.

spirals with a 120° angle between nearest-neighbor moments requires a periodicity of three along the direction of the stripe. With a hexagonal arrangement this is possible only with at least nine atoms per cell. The magnetic structure relieves the frustration caused by the periodic boundary conditions by rotating the moments out of the plane. The configuration is not entirely magnetically compensated, there is a net magnetic moment of $|0.51|\mu_B$ per cell. The total energy is higher than for configuration NCL2 and also higher by 41 meV/atom than for FI2.

We have also explored incommensurate spin-spiral solutions, using a fixed geometry corresponding to configuration NCL1. The resulting solution (see Fig. 11) is a spin spiral with a periodicity of about 18 interatomic distances. The angle of rotation between nearest neighbors along the direction of the stripe is 162°, i.e., this is essentially a long-period modulated AFM configuration. The total energy of the locally stable spin spiral is higher than that of both noncollinear or FI configurations. This shows that a complex relaxation of both geometric and magnetic degrees of freedom is required to achieve a minimum-energy configuration.

3. Vector-field description of the magnetization density

Our investigations are based on a vector-field description of the magnetization which allows for a continuous rotation of the direction of magnetization. It is therefore interesting to analyze the noncollinear magnetic structures in more detail. The graphical representation of the vector field is, however, quite demanding. Hence we show in Fig. 12 only one relatively simple example, the distribution of the local magnetization in a triangular stripe (configuration NCL2 derived from the 3Q starting structure). The three panels show the spatial variation in the absolute magnitude of the magnetization and of the polar and azimuthal angles. The geometry and the orientation of the local magnetic moments for this configuration are shown in Fig. 7(e). This analysis shows that the magnetization vectors remain almost parallel within a sphere around each atom, the rotation of the magnetization

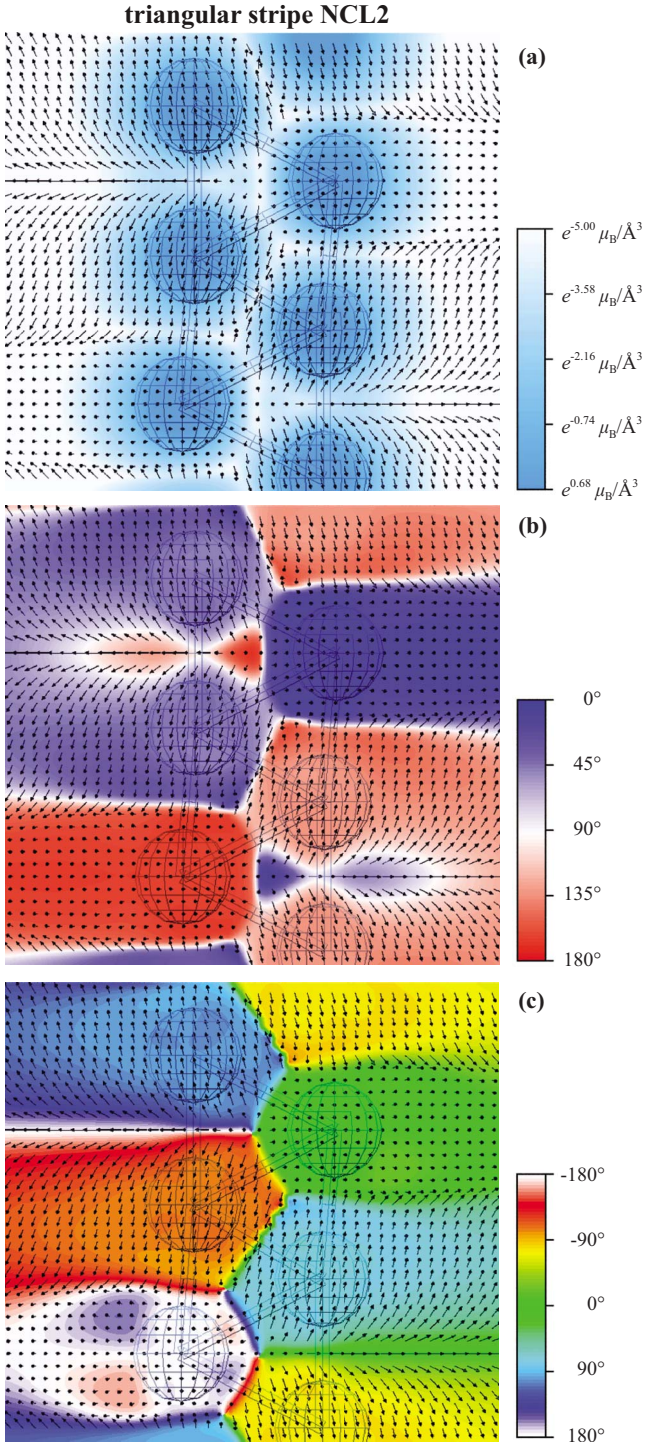

FIG. 12. (Color online) Vector field of the magnetization density in the atomic plane of a triangular stripe of Mn atoms for the noncollinear configuration shown in Fig. 7(e). The small arrows indicate only the direction but not the strength of the local magnetization, projected onto the plane. In part (a) the color coding visualizes the local strength of the magnetization in μ_B (note that the scale is logarithmic), in parts (b) and (c) the color represent the polar and azimuthal angles of the magnetization vector, respectively. Cf. text.

vectors is confined to a transition region representing an atomic analogon to a domain wall. Interestingly, the width of the transition region is rather variable but here the strength of

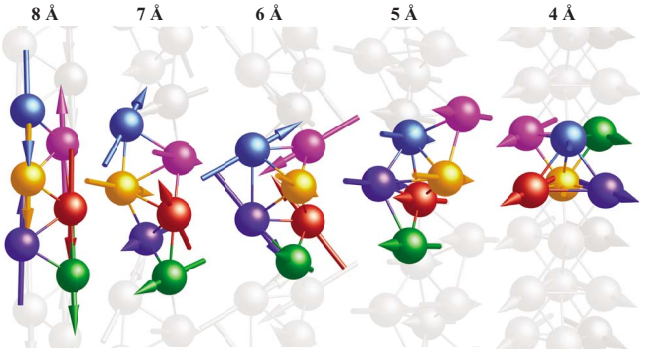

FIG. 13. (Color online) Geometric and magnetic structure in the transition regime from two-dimensional to three-dimensional nanostructures as a function of the height c of the computational cell. Cf. text.

the magnetization is relatively weak. In this configuration the magnetic structure is fully three dimensional, on two of the six atomic sites the magnetization is directed perpendicular to the plane of the stripe, on the remaining four sites the orientation is oblique to the plane. Between two such atoms, the transition region is relatively broad. In the center of the triangles formed by atoms with the same vertical component of the magnetization one even observes an antiparallel orientation of the local magnetization. Graphs of the magnetization fields for the other noncollinear magnetic configurations of the triangular and hexagonal stripes will be published on our website.

D. From stripes to rods

If the compression of the cell is continued beyond the point where a flat triangular stripe represents the equilibrium configuration and a full three-dimensional relaxation is admitted, a continuous transition to three-dimensional nanorod takes place. The stages of this transformation are illustrated in Fig. 13. The starting state is a flat triangular stripe with a slightly noncollinear FI configuration realized for $c=8.5$ Å as shown in Fig. 5. Already at $c=8$ Å a slight puckering of the stripe is observed—interestingly, this allows a nearly parallel alignment of the local magnetic moment. Compression to $c=7$ Å induces a strong buckling of the stripe and a strong rotation of the local moments. At $c=6$ Å a rather regular transitional structure is found, consisting of a stripe of distorted rectangles, each rectangle being capped by another atom. Atoms occupying the short edges of the trapeze couple antiferromagnetically, with an orientation perpendicular to the moments on the other side of the trapeze. The moments of the capping atoms are directed essentially perpendicular to the stripe, with alternating up and down orientations. The net magnetic moment is almost zero, hence this configuration is noncollinear AFM. Compression to $c=5$ Å creates a structure describable in terms of corner-sharing tetrahedra with a nearly collinear AFM configuration. Further compression to $c\sim 4$ Å results in a structure consisting of a stacking of face-sharing distorted octahedra. Alternatively, this structure could also be described in terms of a stacking of distorted antiprisms. The local magnetic moments are slightly canted relative to the axis of the rod, four large magnetic moments point down and two lower moments point up. The resultant magnetic moment per cell is large, hence this configuration is noncollinear FI (details will be given in the following section). Continued compression would lead to a structure in which all six atoms per cell form a nearly planar arrangement, with a periodicity of one along the axis of the nanorod. Although this leads to a further lowering of the total energy, the periodicity imposes rather strict geometric constraints, therefore these structures have not been further analyzed in the present study.

E. Nanorods

The three-dimensional nanostructure described above has been generated by a continuous compression of a triangular stripe. To examine whether this results in the energetically most favorable geometric and magnetic structure, we have investigated also other configurations. The total energies and magnetic moments of the optimized structures are shown in Fig. 14 as a function of the cell height. The first geometry we have tested consists of a stacking of triangular prisms (see Fig. 15). In this case only two collinear AFM configurations

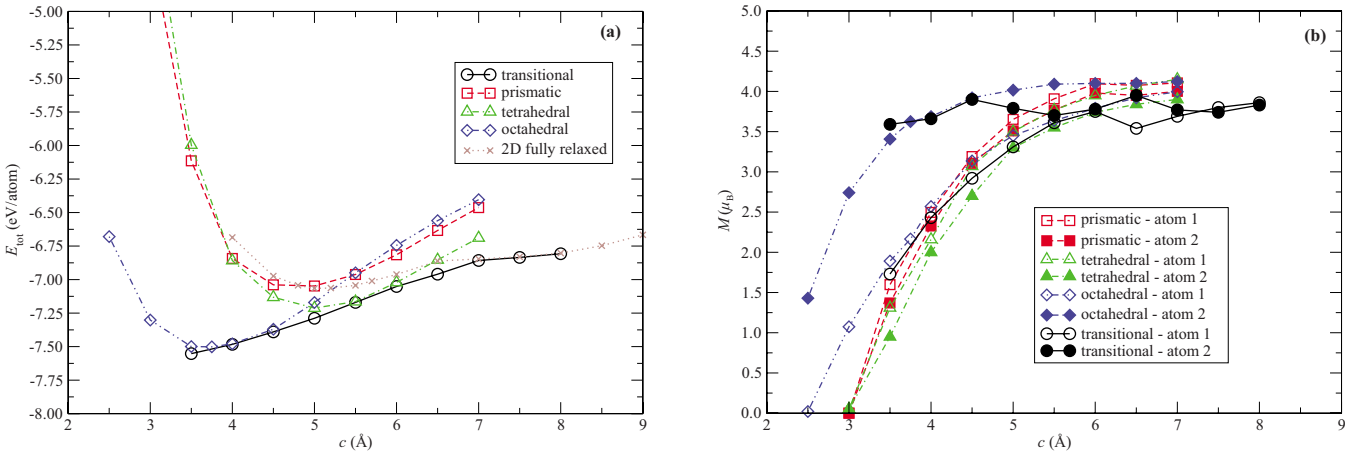

FIG. 14. (Color online) Total energy (a) and magnetic moments (b) of the three-dimensional nanostructures as a function of the height of the cell. Cf. text.

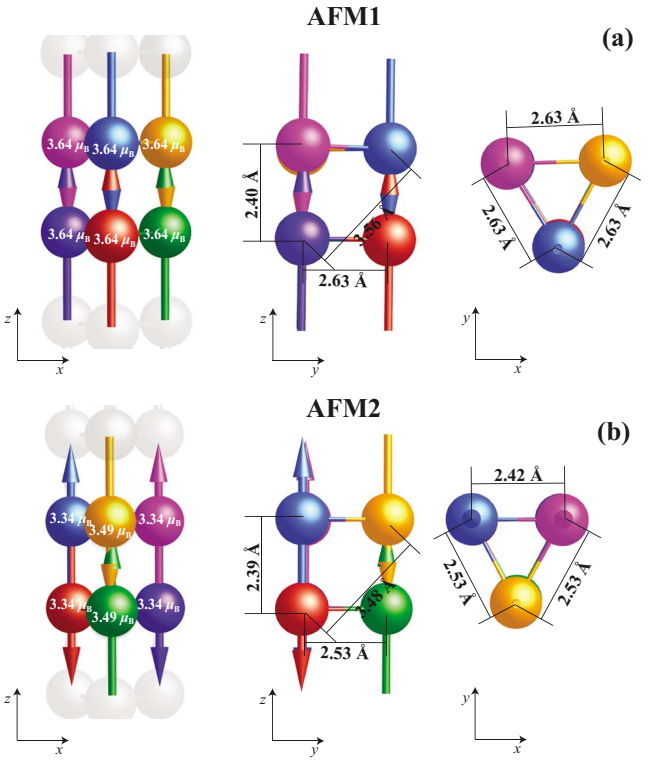

FIG. 15. (Color online) Equilibrium geometric and magnetic configurations of a Mn nanorod formed by a stacking of trigonal antiprisms. Cf. text.

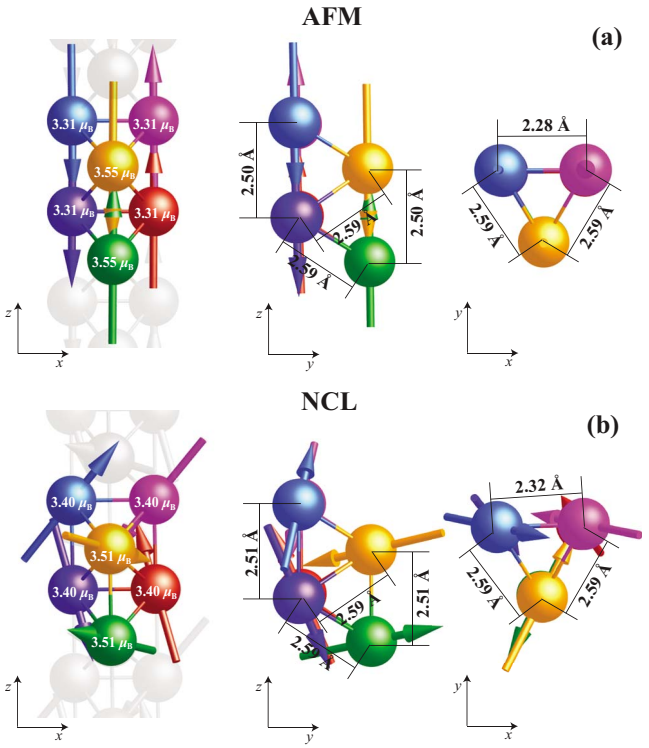

FIG. 16. (Color online) Equilibrium geometric and magnetic configurations of a Mn nanorod in the tetrahedral configuration. Cf. text.

were found to be at least locally stable. Configuration AFM1 consists of equilateral triangles of ferromagnetically coupled atoms, with the direction of the magnetization alternating along the axis of the rods. Distances between antiferromagnetically coupled atoms are shorter (2.40 Å) than the edges of the triangles (2.63 Å), all moments are $3.63\mu_B$. Configuration AFM2 consists of three AFM chains at the edges of the prism. The magnetization direction in one of the chains is phase shifted relative to the other two, the magnetic moments are also slightly larger ($3.49\mu_B$) than along the other two chains ($3.34\mu_B$). The triangular facets consist of isosceles triangles. Configuration AFM2 is 119 meV/atom lower in energy than AFM1.

Because the total energy of a nanorod formed by stacking of trigonal prisms is higher in energy than that of the octahedral configuration resulting from a step-by-step compression of the unit cell, we also tested the intermediate structure shown in Fig. 16 derived by shearing the trigonal prisms along the axis of the rod. This configuration is intermediate between a prismatic and an antiprismatic (or octahedral) configurations, it can also be considered as a chain of corner-sharing distorted tetrahedra. An AFM configuration is realized in the form of two ferromagnetically coupled chains with moments of $\pm 3.31\mu_B$ and one AFM chain carrying slightly larger moments of $3.55\mu_B$. A noncollinear configuration [see Fig. 16(b)] allows to lower the total energy by 30 meV/atom while leaving the geometric structure almost unchanged. However, the total energy is still higher than for the octahedral configuration.

For the octahedral configuration an AFM structure can be realized by aligning the magnetic moments along the direction of the rod. On the trigonal facets shared by the octahedra two atoms carry large ($3.50\mu_B$) ferromagnetically coupled moments while the third atom carries a much lower ($1.18\mu_B$) antiparallel moment. The orientation of the magnetic moments is reversed from one trigonal facet to the next. The basic octahedra forming the nanorod are quite strongly distorted, the edge lengths varying between 2.38 and 2.83 Å (see Fig. 17). If a noncollinear magnetic structure is admitted, the geometric distortion becomes even more pronounced (interatomic distances varying between 2.34 and 2.97 Å), the strongly quenched moments increase from 1.18 to $1.88\mu_B$. Note that the configuration shown in Fig. 17(b) is equivalent to that derived by a step-by-step compression of a triangular stripe at 4 Å (see Fig. 13), the two configurations differ only by a global rotation of the direction of magnetization. Although the local magnetic moments are strongly misaligned, there is a considerable resultant magnetic moment of $7.2\mu_B$ per cell, i.e., this configuration (which is about 6 meV/atom lower in energy than the AFM solution) is noncollinear FI.

We have also tested incommensurate magnetic configurations, based on the geometry of the noncollinear FI state. However, for a three-dimensional nanorod, a spin spiral does not allow enough flexibility to lower the total energy sufficiently. Already in the $q=0$ limit (where the magnetic configuration is identical to AFM), the relatively modest differences in the geometrical structure increase the total energy by about 32 meV/atom. A SS state with $q=0.2\times\frac{2\pi}{c}$ is about 10 meV/atom lower in energy—but this is still distinctly above the AFM and noncollinear (NCL) configurations of

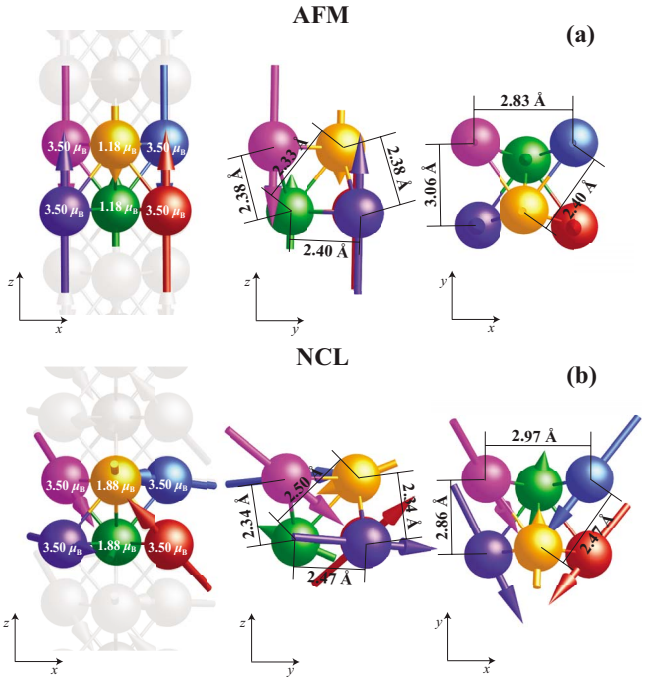

FIG. 17. (Color online) Equilibrium geometric and magnetic configurations of a Mn nanorod in the octahedral configuration. Cf. text.

the octahedral rod. This again confirms that a simultaneous relaxation of both geometric and magnetic degrees of freedom is required.

IV. DISCUSSION AND CONCLUSIONS

Due to recent progress the investigation of the magnetic properties of nanostructures certainly belongs to the frontiers of condensed-matter science. Although thanks to tremendous efforts the properties of FM nanostructures (clusters, chains, and ultrathin films) are now quite well understood, relatively little is known about the behavior of AFM nanostructures. Here the key problem is magnetic frustration, i.e., the impossibility to simultaneously satisfy competing exchange interactions between neighboring atoms. Frustration can be relieved by creating noncollinear magnetic structures, by geometric distortion—or both occurring simultaneously. The resulting structures can be of unprecedented complexity, combining low symmetry of the geometrical structure with magnetic moments aligned on quantization axes changing from atom to atom and continuously rotating in between the atoms. In this paper we have presented detailed spin-density-functional studies of the geometric and magnetic structures of nano-objects formed by Mn atoms under constraints varying from straight monatomic chains over flat two-dimensional stripes to three-dimensional nanorods under varying axial tension. Collinear and noncollinear magnetic structures have been investigated and in addition incommensurate magnetic configurations in the form of spin spirals have been explored. In contrast to previous investigations of free Mn clusters[50] the varying geometrical constraints applied to our nano-objects (periodicity, dimensionality, tension,…) allow to study in detail the interplay between the relaxation of the geometric and magnetic degrees of freedom.

For a Mn monowire, the ground-state configuration is a straight chain with an interatomic distance of 2.41 Å and a high-moment noncollinear structure. Magnetic moments at neighboring atoms are rotated by about 120° such as in the Néel phase of a frustrated triangular antiferromagnet but in addition they are slightly canted relative to a plane through the chain, resulting in a perpendicular net magnetic moment. Calculations admitting an incommensurate spin-spiral structure also predict a rotation of the magnetic moment by 120° between nearest neighbors but the magnetic moments lie in a plane such that the net moment is zero. Noncollinear and spin-spiral solutions are energetically degenerate to within 1 meV/atom. This demonstrates that around the minimum the potential-energy surface in magnetic configuration space is very flat. The noncollinear ground state of a linear Mn chain is at first a surprising result. In contrast to the bulk phases where noncollinearity is caused by the geometric frustration of the nearest-neighbor exchange coupling, the noncollinear antiferromagnetism of a Mn wire is caused by competing short-range and long-range AFM interactions.

If the tension stabilizing a straight chain is gradually reduced (while still imposing a dimensional constraint), two-dimensional stripes of various types are formed, depending on the presence/absence of further constraints. If constant distances between all atoms are imposed, zigzag chains and finally triangular stripes are formed. Remarkably, the "Néel-type" noncollinear arrangement exists over a considerable range of tensions, from $c=14$ to $c\sim 9.5$ Å. At intermediate values of $c\sim 8.5$ Å, however, a collinear AFM configuration is stabilized but the noncollinear structure reappears at further reduced cell height. For triangular stripes in a locally stable state a collinear and a three-dimensional noncollinear AFM configuration with slightly different geometries (see Fig. 5) are energetically almost degenerate (the difference in total energy is 7 meV/atom). Small differences in the atomic geometry lead to significant differences in the hybridization between different $3d$ states and further to different magnetic structures. The closeness of the structural and magnetic energies demonstrates that in this case the frustration caused by both the geometry *and* competing short-range and long-range exchange interactions may be relieved either by a modest geometric distortion or by a strong canting of the magnetic moments.

If the constraint of equal distances along the axis of the nanostructure is dropped, clustering of the atoms in the center of the cell is permitted. The increased freedom to relax the geometry stabilizes collinear magnetic structures all along the transformation to a hexagonal stripe, starting already at $c\sim 10$ Å [cf. Fig. 5(b)]. Determination of the ground state of a hexagonal stripe is complicated by the interplay of geometric and magnetic degrees of freedom and of periodic boundary conditions. The magnetic ground state is collinear FI, with a net magnetic moment of about $1.08\mu_B$/atom along the axis of the stripe. Two noncollinear configurations (also weakly FI) become competitive at slightly reduced distances when the geometric frustrations begin to prevail (see Fig. 7). The occurrence of FI states in hexagonal Mn stripes may be related to FI states

reported for bulk δ-Mn (bcc) and for Mn clusters. Moruzzi and Markus[74] and Sliwko *et al.*[75] found that a FI state is stabilized in expanded bcc Mn in the transition region between CsCl-type and layered AFM states. Mohn *et al.*[15] have argued that this FI state is just the projection of a spin-spiral state on collinear spin-quantization axes. Mn_n clusters with $n=5-40$ have been found to be FI in the experiments of Knickelbein,[28] with average magnetic moments per atom fluctuating between 0.5 and $1\mu_B$/atom. Density-functional calculations[41,48,50] have reached at least semiquantitative agreement with the experiment. Mejia *et al.*[48] have argued that the clusters consist of nanodomains with antiparallel direction of magnetization. In the present case these "nanodomains" of the collinear FI configuration would be simply groups of three atoms with antiparallel moments.

For both the triangular and hexagonal stripes we have also tested incommensurate spin spirals, albeit at a fixed geometry. With this restriction the modest lowering of the total energy realized by adopting an incommensurate structure is not sufficient to produce a competitive low-energy configuration.

If the dimensional constraint is lifted, the transformation to a three-dimensional nanorod sets in already at $c\sim 7$ Å (see Fig. 13). It leads to the formation of a structure describable in terms of a stacking of distorted octahedra. Two configurations with only a modest difference in the atomic geometry but widely different magnetic structures, a collinear AFM and noncollinear FI one, differ by only 6 meV/atom in their total energies. We have also tested two other geometries but these were found to be energetically disfavored. A remarkable feature of both configurations is that for two out of six atoms in the unit cell the magnetic moments are strongly reduced to $1.18\mu_B$ for the collinear and to $1.88\mu_B$ for the noncollinear configuration. The atoms with quenched moments are characterized by short interatomic distances. If the nanorod is further compressed along the axial direction, these atoms become even nonmagnetic [see Fig. 14(b)]. The prismatic and tetrahedral nanorods become even completely nonmagnetic at modest compression. Again, this parallels a pressure-induced transition to a nonmagnetic state in α-Mn which is observed before a pressure-induced transition to equally nonmagnetic ϵ-Mn (hexagonal close-packed) occurs. However, one should keep in mind that for the small unit cells of our nanorods, periodic boundary conditions begin to play an essential role.

The coexistence of atoms in a rather loosely packed environment (large nearest-neighbor distances) with high magnetic moments and atoms in a more tightly packed environment and low magnetic moments is evidently reminiscent of bulk α-Mn, with strongly magnetic and only marginally magnetic moments at inequivalent crystallographic sites. Hence even in the nanostructures the competition between strong chemical binding due to a half-filled d band and the tendency to maximize the magnetic moments according to Hund's rule characteristic for the bulk phases[4,7] begins to be felt. At the other extreme we have the case of the isolated Mn_2 dimer formed by atoms with $S=5/2$, where the occupation of all d states by electrons with parallel spins leads to the formation of a closed d shell and a very weak binding. Clusters and nanostructures fall in between these extremes. In the nanostructures subject to different constraints we find that the possibility to adopt the optimal geometry tends to suppress noncollinearity—or at least to the coexistence of collinear and noncollinear states with different geometrical structures but nearly equal total energies. In clusters external geometrical constraints are absent so that the atoms can adopt optimal geometries. If strong binding leads to closely packed structures characterized by triangular motifs, geometric frustrations can induce noncollinearity—the open question is whether geometrical distortion can again suppress noncollinearity. So far only a few results are available for comparison. Morisato *et al.*[47] have shown that in Mn_5 clusters forming a trigonal bipyramid, collinear and noncollinear FI configurations with different interatomic distances differ by only 10 meV/atom in total energy while for Mn_6 clusters forming different distorted octahedra, a much larger energy difference between the noncollinear ground state and the energetically most favorable collinear configuration (both FI) is reported. Similar results have been found by Longo *et al.*[46,51] but the differences in the geometrical structures have not been documented. The same remark also apply to the study of Kabir *et al.*[50] listing the total energies and magnetic moments for a large series of collinear and noncollinear magnetic isomers of Mn_n clusters with $n=2-10$ and $n=13,15,19$. It is not clear whether for the magnetic isomers the geometry has been relaxed independently or whether the geometries are all the same as determined in earlier work admitting only collinear configurations.

In summary, our investigation has demonstrated that the complexity of the geometric and magnetic properties of Mn nanostructures equals that of the bulk phases. We have demonstrated that a simultaneous relaxation of all structural and magnetic degrees of freedom is required to find the true ground state. Slight differences in the geometry of the clusters (if permitted by the external constraints) are in general found to be as efficient in lowering the total energy as large rotations of the magnetic moments. This shows that the potential-energy surface in magnetic configuration space is relatively flat. As a consequence, an optimization of the magnetic structure is a rather tedious process, it requires different magnetic starting configurations to achieve the true ground state.

Finally we emphasize that our calculations have been based on an unconstrained vector-field description of the magnetization density. The example shown in Fig. 12 demonstrates that the spatial variation in the magnetization density is quite complex. Although the reorientation of the magnetization directions occurs mostly in domains where the magnetization density is rather low, still a precise description is required because these are also precisely the regions where chemical bond formation takes place.

ACKNOWLEDGMENTS

This work has been supported by the Austrian Science Funds under Project No. P19712-NO. M.S. acknowledges support from the Ministry of Education of the Czech Republic under Project No. OC09011.

[1] Y. Ohno, D. K. Young, B. Beschoten, F. Matsukura, H. Ohno, and D. D. Awschalom, Nature (London) **402**, 790 (1999).
[2] K. H. Fischer and J. A. Hertz, *Spin Glasses* (Cambridge University Press, Cambridge, 1991).
[3] Ch. Becker, J. Hafner, and R. Lorenz, J. Magn. Magn. Mater. **157-158**, 619 (1996).
[4] D. Hobbs, J. Hafner, and D. Spišák, Phys. Rev. B **68**, 014407 (2003).
[5] A. C. Lawson, A. C Larson, M. C. Aronson, S. Johnson, Z. Fisk, P. C. Canfield, J. D. Thomson, and R. B. van Dreele, J. Appl. Phys. **76**, 7049 (1994), and references cited therein.
[6] B. Canals and C. Lacroix, Phys. Rev. B **61**, 11251 (2000).
[7] J. Hafner and D. Hobbs, Phys. Rev. B **68**, 014408 (2003).
[8] Y. Endoh and Y. Ishikawa, J. Phys. Soc. Jpn. **30**, 1614 (1971).
[9] S. Surnev, L. Vitali, M. G. Ramsey, F. P. Netzer, G. Kresse, and J. Hafner, Phys. Rev. B **61**, 13945 (2000).
[10] S. Andrieu, H. M. Fischer, M. Piecuch, A. Traverse, and J. Mimault, Phys. Rev. B **54**, 2822 (1996).
[11] J. T. Kohlhepp and W. J. M. de Jonge, Phys. Rev. Lett. **96**, 237201 (2006).
[12] J. T. Kohlhepp, J. Phys. D **40**, 1300 (2007).
[13] T. Oguchi and A. J. Freeman, J. Magn. Magn. Mater. **46**, L1 (1984).
[14] J. Hafner and D. Spišák, Phys. Rev. B **72**, 144420 (2005).
[15] P. Mohn, K. Schwarz, M. Uhl, and J. Kübler, Solid State Commun. **102**, 729 (1997).
[16] H. Fujihisa and K. Takemura, Phys. Rev. B **52**, 13257 (1995).
[17] S. Dennler and J. Hafner, Phys. Rev. B **72**, 214413 (2005).
[18] P. Ferriani, S. Heinze, G. Bihlmayer, and S. Blügel, Phys. Rev. B **72**, 024452 (2005).
[19] P. Ferriani, K. von Bergmann, E. Y. Vedmedenko, S. Heinze, M. Bode, M. Heide, G. Bihlmayer, S. Blügel, and R. Wiesendanger, Phys. Rev. Lett. **101**, 027201 (2008).
[20] C. Grazioli, D. Alfè, S. R. Krishnakumar, S. S. Gupta, M. Veronese, S. Turchini, N. Bonini, A. Dal Corso, D. D. Sarma, S. Baroni, and C. Carbone, Phys. Rev. Lett. **95**, 117201 (2005).
[21] D. H. Lee, J. D. Joannopoulos, J. W. Negele, and D. P. Landau, Phys. Rev. B **33**, 450 (1986).
[22] D. Hobbs and J. Hafner, J. Phys.: Condens. Matter **12**, 7025 (2000).
[23] Ph. Kurz, G. Bihlmayer, K. Hirai, and S. Blügel, Phys. Rev. Lett. **86**, 1106 (2001).
[24] J. C. Tung and G. Y. Guo, Phys. Rev. B **76**, 094413 (2007).
[25] C. Ataca, S. Cahangirov, E. Durgun, Y.-R. Jang, and S. Ciraci, Phys. Rev. B **77**, 214413 (2008).
[26] S. Lounis, P. H. Dederichs, and S. Blügel, Phys. Rev. Lett. **101**, 107204 (2008).
[27] P. Politi and M. G. Pini, Phys. Rev. B **79**, 012405 (2009).
[28] M. B. Knickelbein, Phys. Rev. Lett. **86**, 5255 (2001); Phys. Rev. B **70**, 014424 (2004).
[29] C. W. Bauschlicher, Chem. Phys. Lett. **156**, 95 (1989).
[30] M. R. Pederson, F. Reuse, and S. N. Khanna, Phys. Rev. B **58**, 5632 (1998).
[31] S. K. Nayak and P. Jena, Chem. Phys. Lett. **289**, 473 (1998).
[32] S. K. Nayak, B. K. Rao, and P. Jena, J. Phys.: Condens. Matter **10**, 10863 (1998).
[33] T. M. Briere, M. H. F. Sluiter, V. Kumar, and Y. Kawazoe, Phys. Rev. B **66**, 064412 (2002).
[34] P. Bobadova-Parvanova, K. A. Jackson, S. Srinivas, and M. Horoi, Phys. Rev. A **67**, 061202(R) (2003).
[35] S. N. Khanna, B. K. Rao, P. Jena, and M. Knickelbein, Chem. Phys. Lett. **378**, 374 (2003).
[36] J. Guevara, A. M. Llois, F. Aguilera-Granja, and J. M. Montejano-Carrizales, Phys. Status Solidi B **239**, 457 (2003).
[37] N. O. Jones, S. N. Khanna, T. Baruah, and M. R. Pederson, Phys. Rev. B **70**, 045416 (2004).
[38] B. Wang and Z. Chen, Chem. Phys. Lett. **387**, 395 (2004).
[39] P. Bobadova-Parvanova, K. A. Jackson, S. Srinivas, and M. Horoi, J. Chem. Phys. **122**, 014310 (2005).
[40] S. Yamamoto, H. Tatewaki, H. Moriyama, and H. Nakano, J. Chem. Phys. **124**, 124302 (2006).
[41] M. Kabir, A. Mookerjee, and D. G. Kanhere, Phys. Rev. B **73**, 224439 (2006).
[42] Qing-Min Ma, Zun Xie, Ying Liu, and You-Cheng Li, Chin. Phys. Lett. **24**, 1908 (2007).
[43] G. L. Gutsev, M. D. Mochena, and C. W. Bauschlicher, J. Phys. Chem. A **110**, 9758 (2006).
[44] D. Tzeli, U. Miranda, I. G. Kaplan, and A. Mavridis, J. Chem. Phys. **129**, 154310 (2008).
[45] G. L. Gutsev, M. D. Mochena, C. W. Bauschlicher, W.-J. Zheng, O. C. Thomas, and K. H. Bowen, J. Chem. Phys. **129**, 044310 (2008).
[46] R. C. Longo, E. G. Noya, and L. J. Gallego, J. Chem. Phys. **122**, 226102 (2005).
[47] T. Morisato, S. N. Khanna, and Y. Kawazoe, Phys. Rev. B **72**, 014435 (2005).
[48] J. Mejia-Lopez, A. H. Romero, M. E. Garcia, and J. L. Moran-Lopez, Phys. Rev. B **74**, 140405(R) (2006).
[49] Y. Xie and J. A. Blackman, Phys. Rev. B **73**, 214436 (2006).
[50] M. Kabir, D. G. Kanhere, and A. Mookerjee, Phys. Rev. B **75**, 214433 (2007).
[51] R. C. Longo, M. M. G. Alemany, J. Ferrer, A. Vega, and L. J. Gallego, J. Chem. Phys. **128**, 114315 (2008).
[52] J. Mejia-Lopez, A. H. Romero, M. E. Garcia, and J. L. Moran-Lopez, Phys. Rev. B **78**, 134405 (2008).
[53] D. Hobbs, G. Kresse, and J. Hafner, Phys. Rev. B **62**, 11556 (2000).
[54] M. Zelený, M. Šob, and J. Hafner, Phys. Rev. B **79**, 134421 (2009).
[55] G. Kresse and J. Furthmüller, Phys. Rev. B **54**, 11169 (1996); Comput. Mater. Sci. **6**, 15 (1996).
[56] P. E. Blöchl, Phys. Rev. B **50**, 17953 (1994).
[57] G. Kresse and D. Joubert, Phys. Rev. B **59**, 1758 (1999).
[58] J. P. Perdew, K. Burke, and M. Ernzerhof, Phys. Rev. Lett. **77**, 3865 (1996).
[59] S. H. Vosko, L. Wilk, and M. Nusair, Can. J. Phys. **58**, 1200 (1980).
[60] E. G. Moroni, G. Kresse, J. Hafner and J. Furthmüller, Phys. Rev. B **56**, 15629 (1997).
[61] R. Hafner, D. Spišák, R. Lorenz, and J. Hafner, Phys. Rev. B **65**, 184432 (2002).
[62] M. Eder, J. Hafner, and E. G. Moroni, Phys. Rev. B **61**, 11492 (2000).
[63] C. Herring, in *Magnetism*, edited by G. T. Rado and H. Suhl (Academic, New York, 1966).
[64] L. M. Sandratskii, J. Phys.: Condens. Matter **3**, 8565 (1991); **3**, 8587 (1991).
[65] M. Marsman and J. Hafner, Phys. Rev. B **66**, 224409 (2002).
[66] O. N. Mryasov, A. I. Lichtenstein, L. M. Sandratskii, and V. A. Gubanov, J. Phys.: Condens. Matter **3**, 7683 (1991).

[67] M. Uhl, L. M. Sandratskii, and J. Kübler, J. Magn. Magn. Mater. **103**, 314 (1992).
[68] V. P. Antropov, M. I. Katsnelson, B. N. Harmon, M. van Schilfgaarde, and D. Kusnezov, Phys. Rev. B **54**, 1019 (1996); V. P. Antropov, M. I. Katsnelson, M. van Schilfgaarde, and B. N. Harmon, Phys. Rev. Lett. **75**, 729 (1995).
[69] K. Knöpfle, L. M. Sandratskii, and J. Kübler, Phys. Rev. B **62**, 5564 (2000).
[70] P. Villars and L. D. Calvert, *Pearson's Handbook of Crystallographic Data for Intermetallic Phases*, 2nd ed. (ASM International, Metals Park, OH, 1991).
[71] F. J. Himpsel, Phys. Rev. Lett. **67**, 2363 (1991).
[72] I. Turek, Ch. Becker, and J. Hafner, J. Phys.: Condens. Matter **4**, 7257 (1992).
[73] T. Futschek, J. Hafner, and M. Marsman, J. Phys.: Condens. Matter **18**, 9703 (2006).
[74] V. L. Moruzzi and P. M. Marcus, Phys. Rev. B **38**, 1613 (1988).
[75] V. L. Sliwko, P. Blaha, P. Mohn, and K. Schwarz, Int. J. Quantum Chem. B **7**, 614 (1993).